

Impact of recent $(g - 2)_\mu$ measurement on the light CP-even Higgs scenario in general Next-to-Minimal Supersymmetric Standard Model

Junjie Cao^a, Jingwei Lian^a, Yusi Pan^a, Yuanfang Yue^a, Di Zhang^a

^a *Department of Physics, Henan Normal University, Xinxiang 453007, China*

E-mail: junjiec@alumni.itp.ac.cn, ljwfly@hotmail.com,
panyusi0406@foxmail.com, yueyuanfang@htu.edu.cn,
dz481655@gmail.com

ABSTRACT: The General Next-to-Minimal Supersymmetric Standard Model (GNMSSM) is an attractive theory that is free from the tadpole problem and the domain-wall problem of Z_3 -NMSSM, and can form an economic secluded dark matter (DM) sector to naturally predict the DM experimental results. It also provides mechanisms to easily and significantly weaken the constraints from the LHC search for supersymmetric particles. These characteristics enable the theory to explain the recently measured muon anomalous magnetic moment, $(g - 2)_\mu$, in a broad parameter space that is consistent with all experimental results and at same time keeps the electroweak symmetry breaking natural. This work focuses on a popular scenario of the GNMSSM in which the next-to-lightest CP-even Higgs boson corresponds to the scalar discovered at the Large Hadron Collider (LHC). Both analytic formulae and a sophisticated numerical study show that in order to predict the scenario without significant tunings of relevant parameters, the Higgsino mass $\mu_{tot} \lesssim 500$ GeV and $\tan \beta \lesssim 30$ are preferred. This character, if combined with the requirement to account for the $(g - 2)_\mu$ anomaly, will entail some light sparticles and make the LHC constraints very tight. As a result, this scenario can explain the muon anomalous magnetic moment in very narrow corners of its parameter space.

Contents

1	Introduction	1
2	Theoretical preliminaries	5
2.1	Higgs sector of GNMSSM	6
2.2	Neutralino sector of GNMSSM	9
2.3	Muon g-2 in the GNMSSM	10
3	Explaining Δa_μ in the h_2 scenario of μNMSSM	12
3.1	Research strategy	12
3.2	Key features of the interpretation	15
3.3	LHC constraints	18
4	Explaining Δa_μ in the h_2 scenario of GNMSSM	26
5	Conclusion	27
A	DM-nucleon scattering in the MSSM	28
B	Validation of CERN-EP-2021-059 (ATLAS_2106.01676)	31

1 Introduction

The latest measurement of the muon anomalous magnetic moment $a_\mu \equiv (g - 2)_\mu/2$ announced by the Fermilab National Accelerator Laboratory (FNAL) [1] is in full agreement with the Brookhaven National Laboratory (BNL) E821 result [2]. The combined experimental average is given by Equation (1.1):

$$a_\mu^{\text{Exp}} = 116592061(41) \times 10^{-11}, \quad (1.1)$$

which shows a 4.2σ discrepancy from the Standard Model (SM) theoretical prediction $a_\mu^{\text{SM}} = 116591810(43) \times 10^{-11}$ [3–23], given by Equation (1.2):

$$\Delta a_\mu = a_\mu^{\text{Exp}} - a_\mu^{\text{SM}} = (251 \pm 59) \times 10^{-11}. \quad (1.2)$$

In addition, the Run-1 results in Fermilab also imply that a more thorough analysis in future experiments will most probably substantiate the excess of a_μ in 5σ discovery level. In recent years, this situation has inspired continuous attention to a_μ . In particular, it was widely conjectured that the anomaly may arise from new physics

beyond the SM (see, e.g., Ref. [24] and the references therein). Among a variety of theories that can account for the anomalous magnetic moment, supersymmetry (SUSY) is especially promising due to its elegant structure and natural solutions to many puzzles in the SM, such as the hierarchy problem, the unification of different forces, and the dark matter (DM) mystery [25–28]. Studies of low-energy supersymmetric models have indicated that the source of the significant deviation can be totally or partially contributed to smuon-neutralino or sneutrino-chargino loop effects [24, 29–79].

Although SUSY has multiple theoretical advantages, it has been strongly restricted by DM direct detection (DD) experiments, such as XENON-1T [80, 81] and PandaX-4T [82, 83] experiments, as well as LHC sparticle searches [84–91]. As a consequence, some of its economical realizations become unnatural for electro-weak symmetry breaking in interpreting the anomalous magnetic moment. In the Minimal Supersymmetric Standard Model (MSSM) with R -parity conservation [26, 92–94], the lightest neutralino is usually the lightest supersymmetric particle (LSP), and thus a viable DM candidate. In order to fully account for the DM abundance measured by the Planck experiment [95], it must be Bino-dominated when it is lighter than 1 TeV [96]. In this case, the XENON-1T experiment and the LHC experiments prefer that the magnitude of the Higgsino mass parameter, μ , be larger than about 500 GeV in explaining the discrepancy in the 2σ level [78]. This implies a fine-tuning at the order of 1 % in predicting m_Z [97]. This conclusion may be understood from the features of the DM annihilation mechanisms in the MSSM:

- In the case that the DM co-annihilates with Wino-dominated particles to obtain the measured abundance, the Higgsino mass prefers to be much larger than the DM mass, which was explained in Appendix A of this work. In addition, the SUSY explanation of the deviation together with the results of the LHC search for SUSY can further restrict μ values in a significant way¹.
- In the case that the DM co-annihilates with Higgsino-dominated particles to obtain the measured abundance, the DM DD experiments have required $|\mu|$ to be as large as several TeV, because DM-nucleon scattering rates are enhanced by a factor of $1/(1 - m_{\tilde{\chi}_1^0}^2/\mu^2)^2$ as $m_{\tilde{\chi}_1^0}^2/\mu^2 \rightarrow 1$ (see discussions in Appendix A).

¹In carrying out this study, we also investigated the characteristics of MSSM and Z_3 -NMSSM in a similar way to this work. We found that the co-annihilations with Wino- and Slepton-dominated particles are the main annihilation mechanisms of the bino-dominated DM, i.e., their corresponding Bayesian evidences are the largest in comparison with the other annihilation mechanisms. We also found that the DM preferred to be heavier than about 300 GeV and $|\mu| \gtrsim 500$ GeV when we implemented detailed Monte Carlo simulations for the constraints from the latest LHC searches for electroweakinos. These observations significantly improve the conclusions of [78] and [79], since more LHC analyses were considered carefully.

- In the case that the DM co-annihilates with Sleptons to obtain the measured abundance, the LHC's searches for electroweakinos require Higgsinos to be massive because Wino- and Higgsino-dominated electroweakinos can decay into Sleptons and thus enhance the production rate of lepton signals at the LHC [67].
- In the case that the DM co-annihilates with Squarks or Gluinos to obtain the measured abundance, the LHC's searches for colored sparticles require the DM mass to be heavier than 1 TeV [98].
- In the case that the DM obtains the measured abundance by the SM-like Higgs funnel or Z funnel, the LHC's searches for electroweakinos prefer massive Higgsinos because the DM is relatively light and the LHC's constraints on sparticle mass spectrum are rather strong [99].
- The case in which the DM obtains the measured abundance by the resonance of heavy doublet Higgs bosons is rare. One reason for this is that this case requires significant tuning of SUSY parameters to realize the correlation $|m_{\tilde{\chi}_1^0}| \simeq m_A/2$, where m_A denotes the mass of CP-odd Higgs bosons in MSSM. Another reason is that the LHC's searches for exotic Higgs bosons prefer the bosons to be very massive [100]. Consequently, the DM is also massive.

Next, we consider the Next-to-Minimal Supersymmetric Standard Model with a Z_3 symmetry (Z_3 -NMSSM) [101, 102]. This model extends MSSM by a gauge-singlet Higgs superfield \hat{S} , and has the advantage that either a Bino-dominated (in most physical cases) or a Singlino-dominated neutralino can act as a viable DM candidate [99, 103–114]. The Bino-dominated DM candidate differs from the MSSM prediction mainly in that it could co-annihilate with a Singlino-dominated neutralino to obtain the measured abundance [106]. This situation, however, occurs in very narrow parameter space characterized by $|2\kappa\mu/\lambda| \simeq |M_1|$, moderately large λ and κ , and $|\mu| \gtrsim 300$ GeV [106, 112]. In addition, a_μ^{SUSY} is insensitive to Yukawa coupling λ because the Singlino field has no mixing with Wino and Bino fields, and it does not couple directly to the muon lepton. As a result, the formulae to calculate a_μ^{SUSY} in NMSSM are same as those at the lowest order of the mass-insertion approximation in MSSM [67]. Considering these features, we expected that the Bino-dominated DM case in the Z_3 -NMSSM and MSSM would not show significant differences in explaining the discrepancy. The properties of the Singlino-dominated DM are determined by λ , the Higgsino mass μ (denoted by μ_{tot} in this work), and $\tan\beta$ for a given DM mass [115]. A relatively large λ can increase the DM-nucleon scattering cross-sections, and so far, $\lambda \gtrsim 0.3$ is disfavored by the XENON-1T experiments [112, 115]. This conclusion implies that the traditional DM annihilation channels, $\tilde{\chi}_1^0 \tilde{\chi}_1^0 \rightarrow t\bar{t}, h_s A_s, h A_s$, where t, h, h_s , and A_s denote the top quark, SM-like Higgs boson, and singlet-dominated CP-even and CP-odd Higgs bosons, respectively,

can not be fully responsible for the measured abundance [112]. As a result, the DM is more likely to obtain the abundance by means of the co-annihilation with the Higgsino-dominated particles, which corresponds to a correlated parameter space of $2|\kappa| \simeq \lambda$ with $\lambda \lesssim 0.1$. The Bayesian evidence in this case is heavily suppressed owing to the very narrow parameter space, which entails a certain degree of fine-tuning to meet the DM experiments [115]. In addition, the interpretation of the magnetic moment causes the Z_3 -NMSSM to be further restricted by the updated searches for SUSY at the LHC with $139fb^{-1}$ data. In particular, the region of $\tan\beta \lesssim 30$ in Figure 7 of [99] has been excluded because both the DM and Higgsinos are relatively light. Such a situation, as we will show below, was frequently encountered in this work.

The dilemma of MSSM and Z_3 -NMSSM inspired us to study the general Next-to-Minimal Supersymmetric Standard Model (GNMSSM) [116]. Unlike Z_3 -NMSSM, GNMSSM usually predicts the Singlino-dominated neutralino as a viable DM candidate due to its following specific theoretical feature: the properties of the Singlino-dominated DM are described by λ , μ_{tot} , $m_{\tilde{\chi}_1^0}$, $\tan\beta$, and κ , among which the first four parameters determine the DM couplings to nucleon, and κ mainly dominates the DM couplings to singlet-dominated Higgs bosons [116]. Consequently, singlet-dominated particles $\tilde{\chi}_1^0$, h_s , and A_s can constitute a secluded DM sector, where the measured DM abundance can be achieved by the h_s/A_s -mediated resonant annihilation into SM particles or through the annihilation process of $\tilde{\chi}_1^0\tilde{\chi}_1^0 \rightarrow h_s A_s$ by adjusting the value of κ . Given that this sector interacts with SM matters only through weak singlet-doublet Higgs field mixing, the DM-nucleon scattering rate can be naturally suppressed by $\lambda v/\mu_{tot}$ when λ is small [116]. Since the parameters need no significant tuning to be consistent with the constraints from the DM experiments, the corresponding Bayesian evidence is significantly larger than that for the Bino-dominated DM case [116]. Other characteristics of the theory include that, due to the very weak couplings of the Singlino-dominated DM to other sparticles, heavy sparticles initially prefer to decay into next-to-LSP (NLSP) or next-next-to-LSP (NNLSP). As a result, their decay chains are lengthened and their signals become complicated. In addition, the DM as LSP may be moderately heavy, since the annihilation $\tilde{\chi}_1^0\tilde{\chi}_1^0 \rightarrow h_s A_s$ requires $m_{DM} > (m_{h_s} + m_{A_s})/2$. These features weaken significantly the limitations from the LHC's searches for SUSY. Specifically, in our recent work, we studied a_μ^{SUSY} in a simplified version of GNMSSM, which we called μ -extended NMSSM (μ NMSSM) [67]. We found that, by presuming the DM and LHC experiments are satisfied, μ NMSSM can explain the discrepancy in a broad parameter space where Higgsinos are lighter than about 500 GeV.

In our previous work [67], we considered only the h_1 scenario, in which the lightest CP-even Higgs boson corresponds to the SM-like Higgs boson discovered at the LHC. A typical feature of NMSSM is that the next lightest CP-even Higgs boson may also act as the SM-like Higgs boson, which has been dubbed the h_2 scenario

in the literature. Thus, a full understanding of GNMSSM necessitates the study of the discrepancy in the h_2 scenario. In particular, given that specific configurations of Higgs parameters are needed to predict $m_{h_1} < (m_{h_2} \simeq 125 \text{ GeV})$ and h_2 to be SM-like, it is conceivable that the h_2 scenario suffers tighter experimental constraints than the h_1 scenario². This leaves in doubt the idea that the h_2 scenario can explain the discrepancy. As a result, a careful examination of the experimental constraints on the h_2 scenario is needed, which is the focus of this work.

This work is organized as follows. In Section 2, we briefly introduce the basics of GNMSSM and the SUSY contribution to the moment. In Section 3, we perform a sophisticated scan over the broad parameter space of μ NMSSM, and show the features of the theory in explaining the discrepancy. By using specific Monte Carlo simulations, we also comprehensively study the constraints from the LHC’s searches for SUSY. In Section 4, we concentrate on the GNMSSM, which has much broader parameter space than μ NMSSM, and perform a similar study to those in Section 3. Lastly, we draw conclusions in Section 5.

2 Theoretical preliminaries

It is well-known that the superpotential of the popular Z_3 -NMSSM is given by [101, 102]

$$W_{Z_3\text{-NMSSM}} = W_{\text{Yukawa}} + \lambda \hat{S} \hat{H}_u \cdot \hat{H}_d + \frac{1}{3} \kappa \hat{S}^3, \quad (2.1)$$

where the Yukawa terms W_{Yukawa} are the same as those in MSSM, $\hat{H}_u = (\hat{H}_u^+, \hat{H}_u^0)^T$ and $\hat{H}_d = (\hat{H}_d^0, \hat{H}_d^-)^T$ are $SU(2)_L$ doublet Higgs superfields, and λ, κ are dimensionless couplings coefficient parameterizing the Z_3 -invariant trilinear terms. GNMSSM differs from Z_3 -MSSM in that its superpotential does not respect the Z_3 symmetry, and thus it contains the following most general renormalizable couplings:

$$W_{\text{GNMSSM}} = W_{Z_3\text{-NMSSM}} + \mu \hat{H}_u \cdot \hat{H}_d + \frac{1}{2} \mu' \hat{S}^2 + \xi \hat{S}. \quad (2.2)$$

Historically, the terms characterized by the bilinear mass parameters μ, μ' and the singlet tadpole parameter ξ were introduced to solve the tadpole problem [101, 117] and the cosmological domain-wall problem of Z_3 -NMSSM [118–120], and the ξ -term can be eliminated by shifting the \hat{S} field and redefining the μ parameter [121]³. The bilinear terms could stem from an underlying discrete R symmetry, Z_4^R or Z_8^R ,

²This conclusion may also be understood intuitively as follows: the lightness of h_1 and the premise that h_1 and h_2 are singlet-dominated and SM-like, respectively, lead to the tendency that some parameters in the Higgs sector are relatively small. Consequently, light sparticles are usually predicted. This phenomenon is similar to the well-known fact that the natural result for electroweak-symmetry breaking prefers $|\mu| \lesssim 500 \text{ GeV}$ [97].

³Throughout this work, we adopt this convention consistently.

after supersymmetry breaking, and be naturally at the electroweak scale [118, 121–124]. Note that these extra terms can change the properties of Higgs bosons and neutralinos (in comparison with the Z_3 -NMSSM prediction) and significantly alter the phenomenology of the theory. As emphasized in the introduction, this is one of main motivations of this work.

2.1 Higgs sector of GNMSSM

Corresponding to the potential in Eq. (2.2), the soft-breaking terms of the GNMSSM are given by [101, 102]

$$-\mathcal{L}_{soft} = \left[\lambda A_\lambda S H_u \cdot H_d + \frac{1}{3} A_\kappa \kappa S^3 + m_3^2 H_u \cdot H_d + \frac{1}{2} m_S'^2 S^2 + h.c. \right] + m_{H_u}^2 |H_u|^2 + m_{H_d}^2 |H_d|^2 + m_S^2 |S|^2. \quad (2.3)$$

where H_u , H_d and S denote the scalar components of the Higgs superfields. The soft-breaking mass parameters $m_{H_u}^2$, $m_{H_d}^2$ and m_S^2 can be fixed by solving the conditional equations for minimizing the scalar potential and then expressing them in terms of the vacuum expectation values (vevs) of the scalar fields: $\langle H_u^0 \rangle = v_u/\sqrt{2}$, $\langle H_d^0 \rangle = v_d/\sqrt{2}$ and $\langle S \rangle = v_s/\sqrt{2}$ with $v = \sqrt{v_u^2 + v_d^2} \simeq 246$ GeV. As usual, the ratio of the two Higgs doublet vevs is defined as $\tan \beta \equiv v_u/v_d$, and an effective μ -parameter of MSSM is generated by $\mu_{eff} \equiv \lambda v_s/\sqrt{2}$. Consequently, the Higgs sector is described by ten free parameters: $\tan \beta$, μ_{eff} , the Yukawa couplings λ and κ , the soft-breaking trilinear coefficients A_λ and A_κ , the bilinear mass parameters μ and μ' , and their soft-breaking parameters m_3^2 and $m_S'^2$.

The GNMSSM predicts three CP-even Higgs bosons $h_i = \{h, H, h_s\}$, two CP-odd Higgs bosons $a_i = \{A_H, A_s\}$, and a pair of charged Higgs bosons $H^\pm = \cos \beta H_u^\pm + \sin \beta H_d^\pm$. In the field convention that $H_{SM} \equiv \sin \beta \text{Re}(H_u^0) + \cos \beta \text{Re}(H_d^0)$, $H_{NSM} \equiv \cos \beta \text{Re}(H_u^0) - \sin \beta \text{Re}(H_d^0)$, and $A_{NSM} \equiv \cos \beta \text{Im}(H_u^0) - \sin \beta \text{Im}(H_d^0)$ [125], the elements of the CP-even Higgs boson mass matrix \mathcal{M}_S^2 in the bases $(H_{NSM}, H_{SM}, \text{Re}[S])$ are read as follows in Equations (2.4) [101]:

$$\begin{aligned} \mathcal{M}_{S,11}^2 &= \frac{2[\mu_{eff}(\lambda A_\lambda + \kappa \mu_{eff} + \lambda \mu') + \lambda m_3^2]}{\lambda \sin 2\beta} + \frac{1}{2}(2m_Z^2 - \lambda^2 v^2) \sin^2 2\beta, \\ \mathcal{M}_{S,12}^2 &= -\frac{1}{4}(2m_Z^2 - \lambda^2 v^2) \sin 4\beta, \\ \mathcal{M}_{S,13}^2 &= -\frac{1}{\sqrt{2}}(\lambda A_\lambda + 2\kappa \mu_{eff} + \lambda \mu') v \cos 2\beta, \\ \mathcal{M}_{S,22}^2 &= m_Z^2 \cos^2 2\beta + \frac{1}{2} \lambda^2 v^2 \sin^2 2\beta, \\ \mathcal{M}_{S,23}^2 &= \frac{v}{\sqrt{2}} [2\lambda(\mu_{eff} + \mu) - (\lambda A_\lambda + 2\kappa \mu_{eff} + \lambda \mu') \sin 2\beta], \\ \mathcal{M}_{S,33}^2 &= \frac{\lambda(A_\lambda + \mu') \sin 2\beta}{4\mu_{eff}} \lambda v^2 + \frac{\mu_{eff}}{\lambda} (\kappa A_\kappa + \frac{4\kappa^2 \mu_{eff}}{\lambda} + 3\kappa \mu') - \frac{\mu}{2\mu_{eff}} \lambda^2 v^2, \end{aligned} \quad (2.4)$$

and those for CP -odd Higgs fields in the bases $(A_{\text{NSM}}, \text{Im}(S))$ are given by Equations (2.5):

$$\begin{aligned}\mathcal{M}_{P,11}^2 &= \frac{2[\mu_{eff}(\lambda A_\lambda + \kappa\mu_{eff} + \lambda\mu') + \lambda m_3^2]}{\lambda \sin 2\beta}, \\ \mathcal{M}_{P,22}^2 &= \frac{(\lambda A_\lambda + 4\kappa\mu_{eff} + \lambda\mu') \sin 2\beta}{4\mu_{eff}} \lambda v^2 - \frac{\kappa\mu_{eff}}{\lambda} (3A_\kappa + \mu') - \frac{\mu}{2\mu_{eff}} \lambda^2 v^2 - 2m_S'^2, \\ \mathcal{M}_{P,12}^2 &= \frac{v}{\sqrt{2}} (\lambda A_\lambda - 2\kappa\mu_{eff} - \lambda\mu').\end{aligned}\quad (2.5)$$

The mass eigenstates $h_i = \{h, H, h_s\}$ and $a_i = \{A_H, A_s\}$ are achieved by unitary rotations V and V_P to diagonalize \mathcal{M}_S^2 and \mathcal{M}_P^2 , respectively, as given by Equations (2.6):

$$\begin{aligned}h_i &= V_{hi}^{\text{NSM}} H_{\text{NSM}} + V_{hi}^{\text{SM}} H_{\text{SM}} + V_{hi}^S \text{Re}[S], \\ a_i &= V_{P,a_i}^{\text{NSM}} A_{\text{NSM}} + V_{P,a_i}^S \text{Im}[S].\end{aligned}\quad (2.6)$$

Among these states, h is defined as the scalar state discovered at the LHC, H and A_H represent the doublet-dominated states which prefer to be heavy in the LHC's search for extra Higgs bosons [100], and h_s and A_s denote the singlet-dominated states. For the sake of discussion, these states are also labelled in an ascending mass order, i.e. $m_{h_1} < m_{h_2} < m_{h_3}$, and $m_{A_1} < m_{A_2}$. Thus, $h_s \equiv h_1$ and $h \equiv h_2$ for the h_2 scenario. The mass of the charged Higgs state H^\pm is expressed as Equation (2.7):

$$m_{H^\pm}^2 = \frac{2[\mu_{eff}(\lambda A_\lambda + \kappa\mu_{eff} + \lambda\mu') + \lambda m_3^2]}{\lambda \sin 2\beta} + m_W^2 - \lambda^2 v^2. \quad (2.7)$$

Regarding the input parameters in the Higgs sector, we note that they have been tightly constrained by the LHC Higgs data for the h_2 scenario, especially $\mu_{tot} \equiv \mu + \mu_{eff}$ does not prefer to be excessively large. To illustrate this point, we assume m_{H^\pm} and A_λ to be at most several TeV for natural electroweak symmetry breaking (see the equations to minimize the Higgs potential in [101]), $\tan \beta \gg 1$ to predict a sizable a_μ^{SUSY} , and $\lambda \leq 0.1$ to suppress the DM-nucleon scattering for Singlino-dominated DM case. Then, after integrating out the heavy Higgs fields H_{NSM} and A_{NSM} [106, 125], we obtain the effective mass matrix for CP-even Higgs bosons in the bases $(H_{\text{SM}}, \text{Re}[S])$, as shown in Equations (2.8):

$$\begin{aligned}\bar{\mathcal{M}}_{H_{\text{SM}} H_{\text{SM}}}^2 &\simeq m_Z^2 + \delta_t, & \bar{\mathcal{M}}_{H_{\text{SM}} \text{Re}[S]}^2 &\simeq \mathcal{M}_{S,23}^2 \simeq \sqrt{2} \lambda v \mu_{tot}, \\ \bar{\mathcal{M}}_{\text{Re}[S] \text{Re}[S]}^2 &\simeq \mathcal{M}_{S,33}^2 - \frac{\mathcal{M}_{S,13}^4}{\mathcal{M}_{S,11}^2 - \mathcal{M}_{S,33}^2} \\ &\simeq \frac{\mu_{eff}}{\lambda} (\kappa A_\kappa + \frac{4\kappa^2 \mu_{eff}}{\lambda} + 3\kappa\mu') - \frac{\mu_{tot}}{2\mu_{eff}} \lambda^2 v^2 + \frac{1}{2} \lambda^2 v^2,\end{aligned}\quad (2.8)$$

where δ_t denotes top/stop loop correction to Higgs boson mass, and the singlet-dominated CP-odd Higgs boson mass is given by Equation (2.9):

$$\begin{aligned} m_{A_s}^2 &\simeq \mathcal{M}_{P,22}^2 - \frac{\mathcal{M}_{P,12}^4}{\mathcal{M}_{P,11}^2 - \mathcal{M}_{P,22}^2} \\ &\simeq -\frac{\kappa\mu_{eff}}{\lambda}(3A_\kappa + \mu') - \frac{\mu_{tot}}{2\mu_{eff}}\lambda^2 v^2 + \frac{1}{2}\lambda^2 v^2 - 2m_S'^2. \end{aligned} \quad (2.9)$$

We also obtain the following approximations as shown in Equation (2.10):

$$\begin{aligned} \frac{V_h^S}{V_h^{SM}} &\simeq \frac{\bar{\mathcal{M}}_{H_{SM}Re[S]}^2}{m_h^2 - m_{h_s}^2} \simeq \frac{\sqrt{2}\lambda\mu_{tot}}{m_h^2 - m_{h_s}^2}, \quad V_h^{NSM} \sim 0, \quad V_h^{SM} \simeq \left[1 + \left(\frac{V_h^S}{V_h^{SM}}\right)^2\right]^{-1/2} \sim 1, \\ V_{P,A_s}^{NSM} &\simeq 0, \quad V_{P,A_s}^S \simeq 1. \end{aligned} \quad (2.10)$$

These formulae reveal the following facts:

- Parameters A_λ and m_3 mainly determine the heavy Higgs boson masses, and they have little impact on the other Higgs bosons' mass spectrums.
- m_{h_s} and m_{A_s} depend on parameters λ , κ , μ_{eff} , μ_{tot} , A_κ and μ' . In addition, m_{A_s} also depends on m_S' . This implies that, even when λ , κ , μ_{eff} , μ_{tot} , and μ' are fixed, m_{h_s} and m_{A_s} can still vary freely by the adjustment of A_κ and m_S' , respectively. This situation is different from that of Z_3 -NMSSM, where $\mu_{tot} \equiv \mu_{eff}$, $\mu' = 0$, and $m_S' = 0$, and consequently, the masses of singlet fields are correlated [99].
- The most important feature is that the latest LHC Higgs data have imposed an upper limit of about 40 GeV on $|\lambda\mu_{tot}|$ in the tremendously large $\tan\beta$ limit, since $|\lambda\mu_{tot}|$ may induce a sizable V_h^S . Furthermore, since a small λ is preferred by DM DD experiments in the Singlino-dominated DM case, $|\mu_{eff}|$, $|\mu_{tot}|$ and $|\mu_{tot}/\mu_{eff}|$ in Eq.(2.8) are unlikely to be exceedingly large. Otherwise, strong cancellations among the different terms on the right side of Eq.(2.8) are needed to predict $m_{h_s} < 125$ GeV, which makes the theory fine-tuned.

Given that too many parameters are involved in the Higgs sector, the h_2 scenario is studied using the following strategy. First, we assume the charged Higgs bosons to be very massive by setting $A_\lambda = 2$ TeV and $m_3 = 1$ TeV, following the discussion above. Second, we investigate the characteristics of μ NMSSM, where μ' and m_S' are taken to be zero⁴. This model contains most of the key features of the

⁴Note that μ NMSSM as the most economical realization of GNMSSM could arise from the Z_3 -NMSSM when it was embedded into canonical superconformal supergravity in the Jordan frame, and had applications to the inflation in the early universe [126–130]. This is an interesting realization of supersymmetry in particle physics.

GNMSSM [116], and thus has pedagogical significance. Finally, we concentrate on the GNMSSM by treating μ , μ' and m'_S as variables, and investigate its features in explaining the discrepancy.

2.2 Neutralino sector of GNMSSM

The neutralino sector in the GNMSSM consists of the mixtures among the Bino field \tilde{B} , the Wino field \tilde{W} , the Higgsino fields \tilde{H}_d^0 , \tilde{H}_u^0 and the Singlino field \tilde{S} . Its mass matrix in the basis $(-i\tilde{B}, -i\tilde{W}, \tilde{H}_d^0, \tilde{H}_u^0, \tilde{S})$ takes the the following form [101], as shown in Equation (2.11):

$$M_{\tilde{\chi}^0} = \begin{pmatrix} M_1 & 0 & -m_Z \sin \theta_W \cos \beta & m_Z \sin \theta_W \sin \beta & 0 \\ & M_2 & m_Z \cos \theta_W \cos \beta & -m_Z \cos \theta_W \sin \beta & 0 \\ & & 0 & -\mu_{tot} & -\frac{1}{\sqrt{2}} \lambda v \sin \beta \\ & & & 0 & -\frac{1}{\sqrt{2}} \lambda v \cos \beta \\ & & & & \frac{2\kappa}{\lambda} \mu_{\text{eff}} + \mu' \end{pmatrix}, \quad (2.11)$$

where M_1 and M_2 are gaugino soft-breaking masses, and μ_{tot} represents the Higgsino mass. This matrix can be diagonalized by a rotation matrix N , and subsequently the mass eigenstates are expressed by Equation (2.12):

$$\tilde{\chi}_i^0 = N_{i1}\psi_1^0 + N_{i2}\psi_2^0 + N_{i3}\psi_3^0 + N_{i4}\psi_4^0 + N_{i5}\psi_5^0. \quad (2.12)$$

where $\tilde{\chi}_i^0$ ($i = 1, 2, 3, 4, 5$) are labeled in an ascending mass order. N_{i3} and N_{i4} characterize the \tilde{H}_d^0 and \tilde{H}_u^0 components in $\tilde{\chi}_i^0$, and N_{i5} denotes the Singlino component.

In the case of very massive gauginos and $|m_{\tilde{\chi}_1^0}^2 - \mu_{tot}^2| \gg \lambda^2 v^2$, the following approximations are obtained for the Singlino-dominated $\tilde{\chi}_1^0$ [131–133], given by Equations (2.13):

$$\begin{aligned} \mu' &\simeq m_{\tilde{\chi}_1^0} - \frac{1}{2} \frac{\lambda^2 v^2 (m_{\tilde{\chi}_1^0} - \mu_{tot} \sin 2\beta)}{m_{\tilde{\chi}_1^0}^2 - \mu_{tot}^2} - \frac{2\kappa}{\lambda} \mu_{eff}, \quad N_{11} \sim 0, \quad N_{12} \sim 0, \quad (2.13) \\ \frac{N_{13}}{N_{15}} &= \frac{\lambda v}{\sqrt{2} \mu_{tot}} \frac{(m_{\tilde{\chi}_1^0}/\mu_{tot}) \sin \beta - \cos \beta}{1 - (m_{\tilde{\chi}_1^0}/\mu_{tot})^2}, \quad \frac{N_{14}}{N_{15}} = \frac{\lambda v}{\sqrt{2} \mu_{tot}} \frac{(m_{\tilde{\chi}_1^0}/\mu_{tot}) \cos \beta - \sin \beta}{1 - (m_{\tilde{\chi}_1^0}/\mu_{tot})^2}, \\ N_{15}^2 &\simeq \left(1 + \frac{N_{13}^2}{N_{15}^2} + \frac{N_{14}^2}{N_{15}^2} \right)^{-1} \\ &= \frac{\left[1 - (m_{\tilde{\chi}_1^0}/\mu_{tot})^2 \right]^2}{\left[(m_{\tilde{\chi}_1^0}/\mu_{tot})^2 - 2(m_{\tilde{\chi}_1^0}/\mu_{tot}) \sin 2\beta + 1 \right] \left(\frac{\lambda v}{\sqrt{2} \mu_{tot}} \right)^2 + \left[1 - (m_{\tilde{\chi}_1^0}/\mu_{tot})^2 \right]^2}. \end{aligned}$$

These approximations indicate that the mass of the Singlino-dominated DM is determined by the parameters λ , κ , μ_{eff} , μ_{tot} , and μ' . In particular, λ and κ are two independent parameters in predicting $|m_{\tilde{\chi}_1^0}| < |\mu_{tot}|$. This situation is different from

that of the Z_3 -NMSSM, where $\mu' \equiv 0$, $\mu_{tot} \equiv \mu_{eff}$, and consequently, $|\kappa|$ must be less than $\lambda/2$ to predict the Singlino-dominated neutralino as the LSP [101]. They also indicate that, for fixed $\tan\beta$, the Higgsino compositions in $\tilde{\chi}_1^0$ depend only on λ , μ_{tot} , and $m_{\tilde{\chi}_1^0}$. Therefore, it is convenient to take the three parameters and κ as theoretical inputs in studying the $\tilde{\chi}_1^0$'s properties, where κ determines the interactions among the singlet-dominated particles. This characteristic contrasts with that of the Z_3 -NMSSM, which only needs the three input parameters of λ , μ_{tot} , and any of $m_{\tilde{\chi}_1^0}$ or κ to describe $\tilde{\chi}_1^0$ properties [115]. These differences imply that the singlet-dominated particles may form a secluded DM sector [134], which has the following salient features:

- The Singlino-dominated DM can achieve the correct abundance by the process $\tilde{\chi}_1^0 \tilde{\chi}_1^0 \rightarrow h_s A_s$, through adjusting the value of κ , or by the h_s/A_s -mediated resonant annihilation into SM particles.
- Since the secluded sector communicates with the SM sector only through the weak singlet-doublet Higgs mixing, the interaction between the DM and nucleus is naturally feeble when λ is small.

We added that, even when λ , κ , μ_{eff} and μ_{tot} are fixed, $m_{\tilde{\chi}_1^0}$ can still vary freely through the tuning of μ' . In addition to the process $\tilde{\chi}_1^0 \tilde{\chi}_1^0 \rightarrow h_s A_s$ and h_s/A_s resonant annihilation, the DM has other annihilation channels for obtaining the measured abundance [67], e.g., co-annihilation with Higgsino-dominated electroweakinos and/or sleptons, and resonant Z/h annihilations. Owing to these features, the GNMSSM has a broad parameter space consistent with the current DM experimental results. As a result, it is the Singlino-dominated LSP, instead of the Bino-dominated LSP, that is most favored to be a viable DM candidate.

2.3 Muon g-2 in the GNMSSM

The SUSY source of the muon anomalous magnetic moment a_μ^{SUSY} mainly includes loops with a smuon and a neutralino, as well as those with a muon-type sneutrino and a chargino [29–32]. The one-loop contributions to a_μ^{SUSY} in GNMSSM are given by [30, 67] as Equations (2.14):

$$\begin{aligned}
a_\mu^{\text{SUSY}} &= a_\mu^{\tilde{\chi}^0 \tilde{\mu}} + a_\mu^{\tilde{\chi}^\pm \tilde{\nu}}, \\
a_\mu^{\tilde{\chi}^0 \tilde{\mu}} &= \frac{m_\mu}{16\pi^2} \sum_{i,l} \left\{ -\frac{m_\mu}{12m_{\tilde{\mu}l}^2} (|n_{il}^L|^2 + |n_{il}^R|^2) F_1^N(x_{il}) + \frac{m_{\tilde{\chi}_i^0}}{3m_{\tilde{\mu}l}^2} \text{Re}(n_{il}^L n_{il}^R) F_2^N(x_{il}) \right\}, \\
a_\mu^{\tilde{\chi}^\pm \tilde{\nu}} &= \frac{m_\mu}{16\pi^2} \sum_k \left\{ \frac{m_\mu}{12m_{\tilde{\nu}\mu}^2} (|c_k^L|^2 + |c_k^R|^2) F_1^C(x_k) + \frac{2m_{\tilde{\chi}_k^\pm}}{3m_{\tilde{\nu}\mu}^2} \text{Re}(c_k^L c_k^R) F_2^C(x_k) \right\},
\end{aligned} \tag{2.14}$$

where $i = 1, \dots, 5$, $j = 1, 2$ and $l = 1, 2$ denote the neutralino, chargino and smuon index, respectively. This gives us Equations (2.15):

$$n_{il}^L = \frac{1}{\sqrt{2}} (g_2 N_{i2} + g_1 N_{i1}) X_{l1}^* - y_\mu N_{i3} X_{l2}^*, \quad n_{il}^R = \sqrt{2} g_1 N_{i1} X_{l2} + y_\mu N_{i3} X_{l1}, \quad (2.15)$$

$$c_k^L = -g_2 V_{k1}^c, \quad c_k^R = y_\mu U_{k2}^c,$$

where N is the neutralino mass rotation matrix, X the smuon mass rotation matrix, and U^c and V^c the chargino mass rotation matrices defined by $U^{c*} M_C V^{c\dagger} = m_{\tilde{\chi}^\pm}^{\text{diag}}$. $F(x)$ s are the loop functions of the kinematic variables defined as $x_{il} \equiv m_{\tilde{\chi}_i^0}^2 / m_{\tilde{\mu}_l}^2$ and $x_k \equiv m_{\tilde{\chi}_k^\pm}^2 / m_{\tilde{\nu}_\mu}^2$, and take the following form given by Equations (2.16)–(2.19):

$$F_1^N(x) = \frac{2}{(1-x)^4} [1 - 6x + 3x^2 + 2x^3 - 6x^2 \ln x] \quad (2.16)$$

$$F_2^N(x) = \frac{3}{(1-x)^3} [1 - x^2 + 2x \ln x] \quad (2.17)$$

$$F_1^C(x) = \frac{2}{(1-x)^4} [2 + 3x - 6x^2 + x^3 + 6x \ln x] \quad (2.18)$$

$$F_2^C(x) = -\frac{3}{2(1-x)^3} [3 - 4x + x^2 + 2 \ln x], \quad (2.19)$$

They satisfy $F_1^N(1) = F_2^N(1) = F_1^C(1) = F_2^C(1) = 1$ for the mass-degenerate sparticle case.

In practice, it is instructive to understand the features of a_μ^{SUSY} through the mass insertion approximation [31]. Specifically, for the lowest order of the approximation, the contributions to a_μ^{SUSY} can be classified into four types: "WHL", "BHL", "BHR", and "BLR", where W , B , H , L , and R stands for Wino, Bino, Higgsino, and left-handed and right-handed Smuon fields, respectively. These are from the Feynman diagrams involving $\tilde{W} - \tilde{H}_d$, $\tilde{B} - \tilde{H}_d^0$, $\tilde{B} - \tilde{H}_d^0$, and $\tilde{\mu}_L - \tilde{\mu}_R$ transitions, respectively, and take the following form [31, 33, 34] given by Equations (2.20)–(2.23):

$$a_{\mu, \text{WHL}}^{\text{SUSY}} = \frac{\alpha_2}{8\pi} \frac{m_\mu^2 M_2 \mu_{\text{tot}} \tan \beta}{m_{\tilde{\nu}_\mu}^4} \left\{ 2f_C \left(\frac{M_2^2}{m_{\tilde{\nu}_\mu}^2}, \frac{\mu_{\text{tot}}^2}{m_{\tilde{\nu}_\mu}^2} \right) - \frac{m_{\tilde{\nu}_\mu}^4}{m_{\tilde{\mu}_L}^4} f_N \left(\frac{M_2^2}{m_{\tilde{\mu}_L}^2}, \frac{\mu_{\text{tot}}^2}{m_{\tilde{\mu}_L}^2} \right) \right\}, \quad (2.20)$$

$$a_{\mu, \text{BHL}}^{\text{SUSY}} = \frac{\alpha_Y}{8\pi} \frac{m_\mu^2 M_1 \mu_{\text{tot}} \tan \beta}{m_{\tilde{\mu}_L}^4} f_N \left(\frac{M_1^2}{m_{\tilde{\mu}_L}^2}, \frac{\mu_{\text{tot}}^2}{m_{\tilde{\mu}_L}^2} \right), \quad (2.21)$$

$$a_{\mu, \text{BHR}}^{\text{SUSY}} = -\frac{\alpha_Y}{4\pi} \frac{m_\mu^2 M_1 \mu_{\text{tot}} \tan \beta}{m_{\tilde{\mu}_R}^4} f_N \left(\frac{M_1^2}{m_{\tilde{\mu}_R}^2}, \frac{\mu_{\text{tot}}^2}{m_{\tilde{\mu}_R}^2} \right), \quad (2.22)$$

$$a_{\mu, \text{BLR}}^{\text{SUSY}} = \frac{\alpha_Y}{4\pi} \frac{m_\mu^2 M_1 \mu_{\text{tot}} \tan \beta}{M_1^4} f_N \left(\frac{m_{\tilde{\mu}_L}^2}{M_1^2}, \frac{m_{\tilde{\mu}_R}^2}{M_1^2} \right), \quad (2.23)$$

where the loop functions are given by

$$f_C(x, y) = \frac{5 - 3(x+y) + xy}{(x-1)^2(y-1)^2} - \frac{2 \ln x}{(x-y)(x-1)^3} + \frac{2 \ln y}{(x-y)(y-1)^3}, \quad (2.24)$$

$$f_N(x, y) = \frac{-3 + x + y + xy}{(x-1)^2(y-1)^2} + \frac{2x \ln x}{(x-y)(x-1)^3} - \frac{2y \ln y}{(x-y)(y-1)^3}, \quad (2.25)$$

and they satisfy $f_C(1, 1) = 1/2$ and $f_N(1, 1) = 1/6$. Note that the Singlino field \tilde{S} can also enter the insertions. Because both the $\tilde{W} - \tilde{S}$ and $\tilde{B}^0 - \tilde{S}$ transitions and the $\tilde{\mu}\tilde{S}\tilde{\mu}_{L,R}$ couplings vanish, the Singlino field only appears in the "WHL", "BHL" and "BHR" loops by two more insertions at the lowest order, which correspond to the $\tilde{H}_d^0 - \tilde{S}$ and $\tilde{S} - \tilde{H}_d^0$ transitions in the neutralino mass matrix in Eq. (2.11). Since a small λ is preferred by the DM physics, the Singlino-induced contributions are never significant [67]. Although in this case the GNMSSM prediction of a_μ^{SUSY} is roughly the same as that of the MSSM, except that the μ parameter of the MSSM should be replaced by μ_{tot} , the two models predict different DM physics and different sparticle signals at the LHC. Thus, they are subject to different theoretical and experimental constraints. It should also be noted that, although there is a prefactor of the Higgsino mass μ in the expression of the "WHL", "BHL", and "BHR" contributions, the involved loop functions approach zero with the increase of $|\mu|$, and consequently these contributions depend on μ in a complex way. By focusing on several typical patterns of sparticle mass spectrum with a positive μ , we found that the "WHL" contribution decreases monotonously as μ increases, while the magnitude of the "BHL" and "BHR" contributions increases when μ is significantly smaller than the slepton mass and decreases when μ is larger than the slepton mass. In addition, the "WHL" contribution is usually much larger than the other contributions if $\tilde{\mu}_L$ is not significantly heavier than $\tilde{\mu}_R$.

3 Explaining Δa_μ in the h_2 scenario of μNMSSM

3.1 Research strategy

This sector focuses on the h_2 scenario of μNMSSM . In order to analyze its characteristics in explaining the discrepancy, the following parameter space was scanned by MultiNest algorithm [135]:

$$\begin{aligned} 0 \leq \lambda \leq 0.75, \quad |\kappa| \leq 0.75, \quad 1 \leq \tan \beta \leq 60, \\ |M_1| \leq 1.5 \text{ TeV}, \quad 100 \text{ GeV} \leq M_2 \leq 1.5 \text{ TeV}, \quad -5 \text{ TeV} \leq A_t \leq 5 \text{ TeV}, \\ |\mu| \leq 1 \text{ TeV}, \quad 100 \text{ GeV} \leq \mu_{\text{tot}} \leq 1 \text{ TeV}, \quad |A_\kappa| \leq 1 \text{ TeV}, \\ 100 \text{ GeV} \leq m_{\tilde{\mu}_L} \leq 1 \text{ TeV}, \quad 100 \text{ GeV} \leq m_{\tilde{\mu}_R} \leq 1 \text{ TeV}, \end{aligned} \quad (3.1)$$

where the flat prior distribution was chosen for all input parameters and the active point number, n_{live} , was set to be 6000⁵. Other dimensional parameters that are

⁵In the MultiNest algorithm, the active points are used to determine the iso-likelihood contours in each iteration of sampling. Note that **the results obtained by this algorithm has statistical significance.**

unimportant to this study were fixed at 2 TeV, and include SUSY parameters for the first and third generation sleptons, three generation squarks, and gluinos. In numerical calculations, the model file of GNMSSM was constructed using the package **SARAH-4.14.3** [136–139]. Particle mass spectra and low-energy observables, such as a_μ^{SUSY} and B-physics observables, were generated by the codes **SPheno-4.0.4** [140, 141] and **FlavorKit** [142]. The DM abundance and direct/indirect detection cross-sections were calculated by the package **MicrOMEGAs-5.0.4** [143–148]. The likelihood function used to guide the scan mainly contains the value of a_μ^{SUSY} [67], and it takes the following form, given by Equation (3.2):

$$\mathcal{L} = \begin{cases} \exp \left[-\frac{1}{2} \left(\frac{a_\mu^{\text{SUSY}} - 2.51 \times 10^{-9}}{5.9 \times 10^{-10}} \right)^2 \right], & \text{if restrictions satisfied;} \\ \exp[-100], & \text{if restrictions unsatisfied,} \end{cases} \quad (3.2)$$

where the restrictions on each sample include:

1. DM relic abundance, $0.096 \leq \Omega h^2 \leq 0.144$. In implementing this constraint, the central value of the Planck-2018 data, $\Omega h^2 = 0.120$ [149], was used, and a theoretical uncertainty of 10% in abundance calculation was assumed.
2. DM direct and indirect detections. Specifically, the SI and SD DM-nucleon scattering cross-sections should be lower than the bounds from the XENON-1T experiments [150, 151], and the DM annihilation rate at present time should be consistent with dwarf galaxies observations from Fermi-LAT collaboration [152]. The method suggested in [153] was adopted in studying the latter constraint.
3. Higgs data fit. The properties of the next lightest CP-even Higgs boson h_2 (also denoted by h throughout this work) should be consistent at the 95% confidence level with corresponding data obtained by ATLAS and CMS collaborations. This condition was checked with the code **HiggsSignal-2.2.3** [154] by requiring the sample's p value to be larger than 0.05.
4. Direct searches for extra Higgs bosons at LEP, Tevatron and LHC. This requirement was examined by the code **HiggsBounds-5.3.2** [155].
5. Some B-physics observations. Specifically, the branching ratios of $B_s \rightarrow \mu^+ \mu^-$ and $B \rightarrow X_s \gamma$ should agree with their experimental measurements, which were summarized in [156] at the 2σ level.
6. LHC searches for SUSY. In order to explain the discrepancy, the electroweakinos and sleptons in the GNMSSM can not be excessively heavy. Thus, they will be produced at the LHC to generate multi-lepton signals. The code

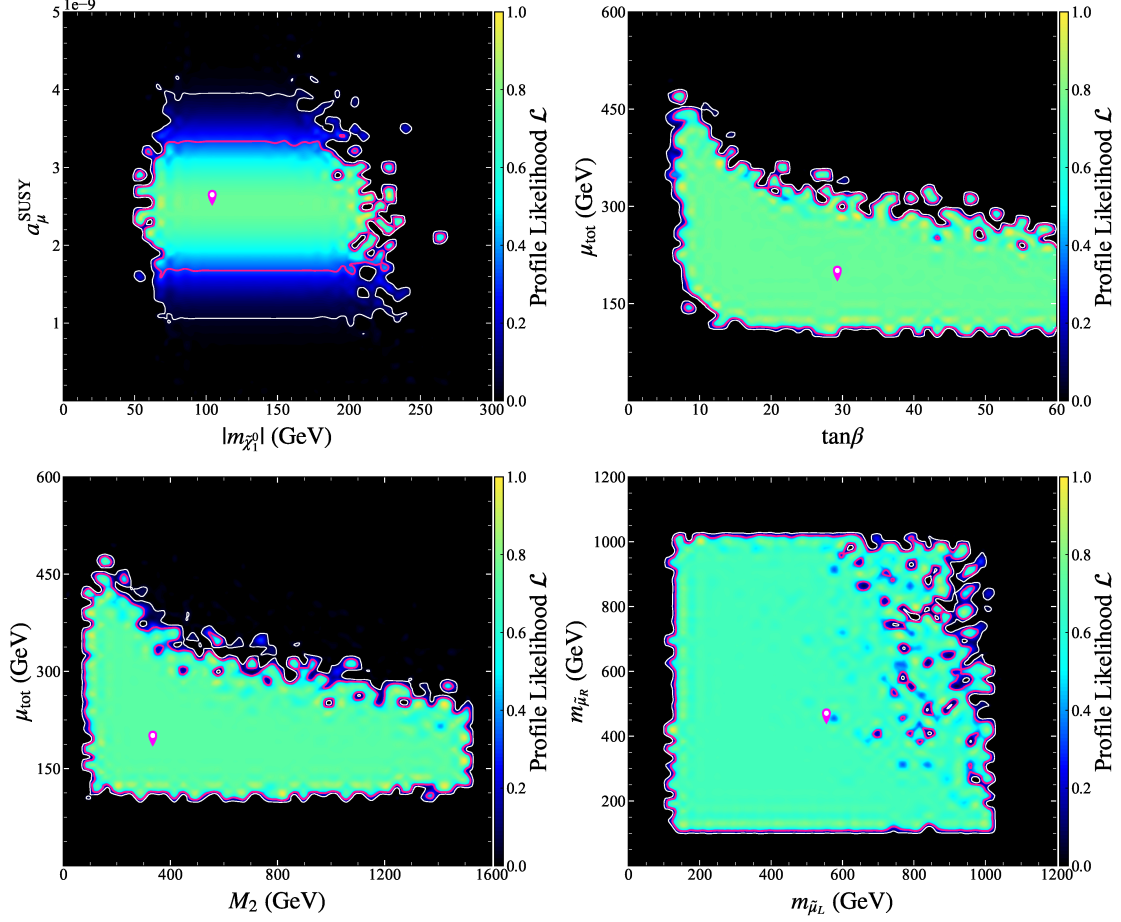


Figure 1. Two-dimensional profile likelihood maps of the function \mathcal{L} in Eq. (3.2) projected onto $|m_{\tilde{\chi}_1^0}| - a_{\mu}^{\text{SUSY}}$, $\tan\beta - \mu_{\text{tot}}$, $M_2 - \mu_{\text{tot}}$, and $m_{\tilde{\mu}_L} - m_{\tilde{\mu}_R}$ planes. Pink and white contour lines enclose 1σ and 2σ confidence regions, respectively. The best point is marked by the pin symbol, and it is located at $\tan\beta \simeq 30$, $m_{\tilde{\chi}_1^0} \simeq 103$ GeV, $\mu_{\text{tot}} \simeq 210$ GeV, $M_2 \simeq 330$ GeV, $m_{\tilde{\mu}_L} \simeq 470$ GeV, and $m_{\tilde{\mu}_R} \simeq 550$ GeV.

SModelS-2.1.1 [157] was used to set limits on the signals in some simple topology cases. Sophisticated study of the constraints will be carried out in subsection 3.3, using the package CheckMATE-2.0.29 [158–160].

7. Vacuum stability for the scalar potential consisting of the Higgs fields and the last two generation slepton fields. This condition was checked by the Vevacious code [161, 162], and its effect on the GNMSSM was recently discussed in [67].

In presenting the results, two-dimensional profile likelihood (PL) for the function \mathcal{L} in Eq.(3.2) was used. It is defined by what follows in Equation (3.3): [163]

$$\mathcal{L}(\Theta_A, \Theta_B) = \max_{\Theta_1, \dots, \Theta_{A-1}, \Theta_{A+1}, \dots, \Theta_{B-1}, \Theta_{B+1}, \dots} \mathcal{L}(\Theta), \quad (3.3)$$

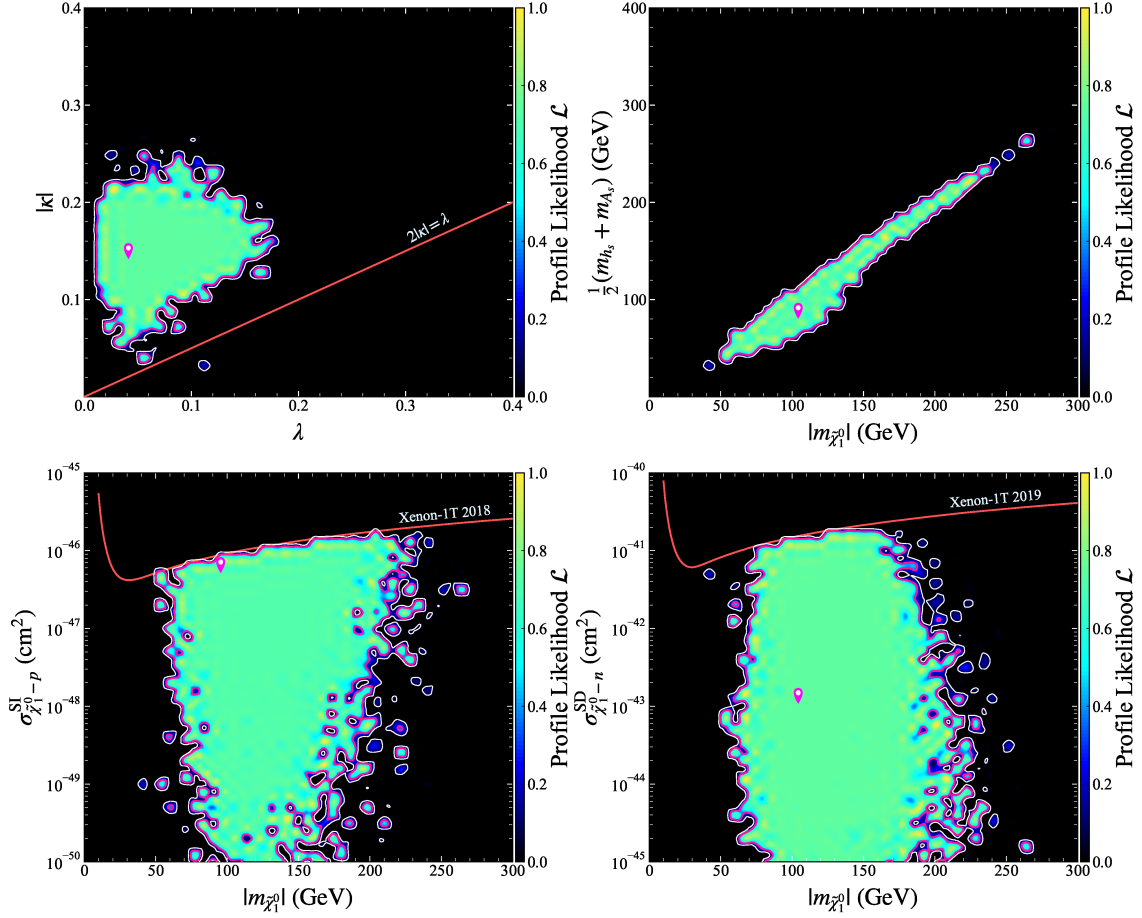


Figure 2. Same as Fig. 1, but on the $\lambda - |\kappa|$, $|m_{\tilde{\chi}_1^0}| - \frac{1}{2}(m_{h_s} + m_{A_s})$, $|m_{\tilde{\chi}_1^0}| - \sigma_n^{\text{SD}}$ and $|m_{\tilde{\chi}_1^0}| - \sigma_p^{\text{SI}}$ planes, respectively.

where $\Theta_i (i = 1, 2, \dots)$ denote the input parameters, $\Theta_{A,B}$ are the variables of interest, and the maximization of $\mathcal{L}(\Theta_A, \Theta_B)$ is achieved by scanning the parameters other than Θ_A and Θ_B . Related quantities includes 1σ and 2σ confidence intervals (CI), and the χ^2 function defined by $\chi^2 \equiv -2\ln\mathcal{L}(\Theta_A, \Theta_B)$. These statistical measures were briefly introduced in [163], and they reflect the capability of the theory to explain the discrepancy.

3.2 Key features of the interpretation

All samples obtained in the scan were projected onto different parameter planes to show two-dimensional PLs, which could reveal the underlying physics of the h_2 scenario. Fig. 1 illustrates that the scenario can interpret the discrepancy in a broad parameter space. Specifically, the upper left panel indicates that the best point predicts $a_\mu^{\text{SUSY}} = 25.1 \times 10^{-10}$, which means $\chi_{\text{Best}}^2 = 0$, $\chi^2 \leq 2.3$ for 1σ CI and $\chi^2 \leq 6.18$ for 2σ CIs. In term of a_μ^{SUSY} , the χ^2 ranges correspond to $16.2 \times 10^{-10} \leq a_\mu^{\text{SUSY}} \leq 34.0 \times 10^{-10}$ and $10.4 \times 10^{-10} \leq a_\mu^{\text{SUSY}} \leq 39.8 \times 10^{-10}$, respectively. The

upper right panel shows that the maximum reach of μ_{tot} decreases monotonously with the increase of $\tan\beta$, and it is about 500 GeV (260 GeV) for $\tan\beta = 10$ ($\tan\beta = 60$). The reason for such a behavior is that, in the case of a relatively small $\tan\beta$, the second term in $\mathcal{M}_{S,23}^2$ of Eq. (2.4) is sizable, and can cancel the first term to suppress V_h^S , which is preferred by LHC Higgs data. As $\tan\beta$ increases, the cancellation effect becomes weak since the second term is suppressed by $\sin 2\beta$, and tighter constraints are set on μ_{tot} ⁶. Moreover, analyzing the posterior probability of the scan results indicates that the scenario prefers small $\tan\beta$ region. Thus, most samples obtained in the scan predict $\tan\beta \lesssim 30$.

The lower left and right panels of Fig. 1 depict the ranges of M_2 , $\tilde{\mu}_L$, and $\tilde{\mu}_R$, which are determined by a_μ^{SUSY} in Eqs. (2.20-2.23). They show that M_2 may be as large as 1.5 TeV, and $\tilde{\mu}_L$ and $\tilde{\mu}_R$ may be as large as 1 TeV. The lower left panel also exhibits that the mass of chargino $\tilde{\chi}_1^\pm$ is less than about 350 GeV. It should be noted that the ranges of M_2 and $\tilde{\mu}_L$ depend strongly on the value of $\tan\beta$. For example, assuming that the theory explains the discrepancy of Δa_μ at 1σ level, it was found that M_2 and $\tilde{\mu}_L$ must be less than about 400 GeV and 350 GeV, respectively, for $\tan\beta = 10$. The upper bounds become 1.2 TeV and 700 GeV for $\tan\beta = 20$, and 1.4 TeV and 1 TeV for $\tan\beta = 27$. By contrast, $m_{\tilde{\chi}_1^0}$ and $\tilde{\mu}_R$ are not sensitive to $\tan\beta$, e.g., $m_{\tilde{\chi}_1^0}$ and $\tilde{\mu}_R$ may vary in the range of $50 \text{ GeV} \lesssim m_{\tilde{\chi}_1^0} \lesssim 250 \text{ GeV}$ and $100 \text{ GeV} \lesssim \tilde{\mu}_R \lesssim 1 \text{ TeV}$ for any value of $\tan\beta$. The basic reason for the phenomenon is that the WHL contribution to a_μ^{SUSY} is usually the dominant one. It depends on M_2 , μ_{tot} , and $\tilde{\mu}_L$, and is in particular proportional to $\tan\beta$. Therefore, when $\tan\beta$ is relatively small, the involved SUSY particles must be moderately light to predict a sizable a_μ^{SUSY} . As a result, the left sides of the lower panels usually correspond to a relatively small $\tan\beta$, and the right sides correspond to a large $\tan\beta$.

Fig. 2 focuses on the DM physics of the h_2 scenario, which involves the parameters λ , κ , μ_{tot} , and the masses of singlet-dominated particles, i.e., $m_{\tilde{\chi}_1^0}$, m_{h_s} and m_{A_s} . It reveals the following features:

- $2m_{\tilde{\chi}_1^0} > m_{h_s} + m_{A_s}$ for most of the parameter areas (see the upper right panel), which implies that in the early universe, the Singlino-dominated DM might annihilate into the singlet-dominated Higgs bosons h_s and A_s . As pointed out in [116], this annihilation proceeded by the s-channel exchange of Z boson

⁶Throughout this work, A_λ is fixed at 2 TeV. If a larger A_λ , e.g., $A_\lambda = 10 \text{ TeV}$, was taken, it was found that $\tan\beta$ tended to become larger, while $|\mu_{tot}|$ and λ tended to be smaller [164]. This tendency is needed to suppress $\mathcal{M}_{S,23}^2$ and $\mathcal{M}_{S,33}^2$ in Eq.(2.4) simultaneously. In addition, the Bayesian evidence of the scenario decreases significantly as A_λ increases [164], which means that setting a large A_λ will cause a more subtle parameter tuning to obtain $m_{h_1} \lesssim 125 \text{ GeV}$ and correct electroweak symmetry breaking. In brief, even when A_λ is treated as a variable in studying the parameter space, the natural realization of the h_2 scenario to interpret the anomaly in the GNMSSM, as suggested by this work, has been tightly limited. This conclusion was verified by our alternative scans.

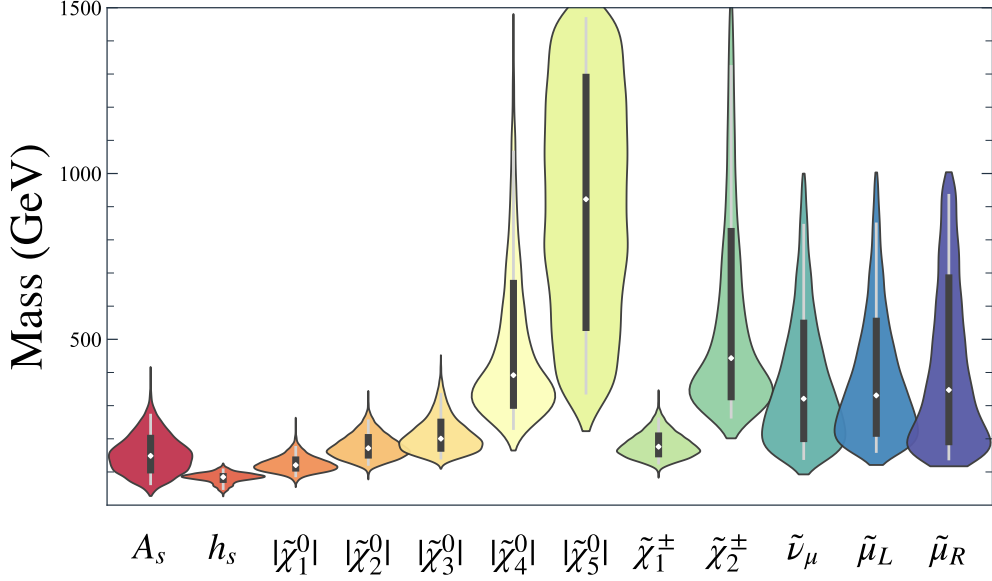


Figure 3. Violin diagrams showing the mass distributions of the singlet Higgs bosons, the electoweakinos, and μ -type sparticles. Smuons are labeled by their dominated component. The violins are scaled by count. The thick vertical bar in the center represents the interquartile range with the white dot denoting the median, and the long vertical line indicates the 95% confidence interval.

and CP-odd Higgs bosons and the t -channel exchange of neutralinos. If the t -channel contribution to the annihilation rate was much larger than the s -channel contribution, $|\kappa| \simeq 0.15 \times (m_{\tilde{\chi}_1^0}/300 \text{ GeV})^{1/2}$ could predict the measured abundance, while if the interference of the two contributions was significantly constructive/deconstructive, a smaller/larger $|\kappa|$ could be fully responsible for the abundance. Given that $0.05 \lesssim |\kappa| \lesssim 0.25$ on the upper left panel, we infer that the process played an important role in determining the abundance. In addition, it was verified in fewer cases that $2m_{\tilde{\chi}_1^0} < m_{h_s} + m_{A_s}$ and/or $|\kappa| \lesssim 0.1$, so that the DM obtained the measured abundance mainly by co-annihilating with the Higgsino-dominated electoweakinos or μ -type sleptons.

- The SI and SD cross-sections of DM-nucleon scattering may be as low as 10^{-50} cm^2 and 10^{-45} cm^2 , respectively (see the lower left and right panels). The SD scattering proceeds only through the Z -mediated Feynman diagram, and the rate is proportional to $(\lambda v/\mu_{tot})^4$ [116]. Thus, it is a small λ , e.g., $\lambda \sim \mathcal{O}(0.01)$, that is responsible for the low SD cross-section (see the upper left panel). By contrast, the SI scattering is induced by three CP-even Higgs bosons, and it is the cancellation of h - and h_s -mediated contributions that mainly accounts for the small SI cross section [115].

The DM physics in the h_2 scenario differs from those of the h_1 scenario, which

were presented in Fig.2 of [67], in three aspects. The first is that the DM is relatively light, i.e., $50 \text{ GeV} \lesssim m_{\tilde{\chi}_1^0} \lesssim 250 \text{ GeV}$ for the h_2 scenario and $150 \text{ GeV} \lesssim m_{\tilde{\chi}_1^0} \lesssim 650 \text{ GeV}$ for the h_1 scenario. Two reasons may explain this phenomenon. One is that $|m_{\tilde{\chi}_1^0}|$ must be less than μ_{tot} , and as shown in Fig. 1, a moderately small μ_{tot} is experimentally preferred for the h_2 scenario. The other reason is that $|m_{\tilde{\chi}_1^0}|$ must be larger than $(m_{h_s} + m_{A_s})/2$ for most cases to proceed to the annihilation $\tilde{\chi}_1^0 \tilde{\chi}_1^0 \rightarrow h_s A_s$. A relatively light $\tilde{\chi}_1^0$ can meet this condition in the h_2 scenario (see the previous discussions). The second one is that $|\kappa|$ is less than 0.25 in the h_2 scenario, while it is less than 0.4 in the h_1 scenario. The underlying reason for this is that a smaller $|\kappa|$ can be fully responsible for the measured abundance in the h_2 scenario. The last aspect is that λ in the h_2 scenario may reach about 0.2, while it is at most 0.1 in the h_1 scenario. This is because the cancellation effect in the SI scattering is usually significant in the h_2 scenario, and consequently, a larger λ is still allowed by DM DD experiments.

In Fig. 3, the mass distributions of the singlet-dominated Higgs states and the SUSY particles relevant to a_μ^{SUSY} are shown by a series of violin plots, which combines the advantages of the box plot and probability density distribution plot [165]. This figure shows that all SUSY particles except for $\tilde{\chi}_5^0$ tend to be lighter than 500 GeV, and in particular, $\tilde{\chi}_2^0$, $\tilde{\chi}_3^0$, and $\tilde{\chi}_1^\pm$ are lighter than 500 GeV for nearly all samples obtained in the scan. The fundamental reason for the phenomenon, besides the explanation presented before, arises from the fact that a low $\tan \beta$ is preferred to predict the h_2 scenario. This tendency, once combined with the requirement of a sizable a_μ^{SUSY} , will necessitate light SUSY particles⁷. Given that these electroweakinos can be richly produced at the LHC, they have been restricted by searching for multi-lepton signals. This issue will be intensively studied in the following.

3.3 LHC constraints

To comprehensively study the constraints from the LHC search for sparticles on the obtained parameter points, the following processes were analyzed in the Monte Carlo (MC) event simulation as given by Equations (3.4)⁸:

$$\begin{aligned}
pp &\rightarrow \tilde{\chi}_i^0 \tilde{\chi}_j^\pm, & i = 2, 3, 4, 5; & \quad j = 1, 2 \\
pp &\rightarrow \tilde{\chi}_i^\pm \tilde{\chi}_j^\mp, & i, j = 1, 2; \\
pp &\rightarrow \tilde{\chi}_i^0 \tilde{\chi}_j^0, & i, j = 2, 3, 4, 5; \\
pp &\rightarrow \tilde{\mu}_i \tilde{\mu}_j, & i, j = 1, 2;
\end{aligned} \tag{3.4}$$

In the calculation, the cross-sections of $\sqrt{s} = 13 \text{ TeV}$ were obtained at the next-to-leading order (NLO) by the package Prospino2 [166]. The MC events were generated

⁷Without the a_μ^{SUSY} requirement, $\tilde{\chi}_1^0$ may be very massive (e.g., $|m_{\tilde{\chi}_1^0}| > 300 \text{ GeV}$ [116]). In this case, the LHC constraints are significantly weakened.

⁸In the compressed spectrum case, relevant processes with additional jets were also considered in the simulations.

Table 1. Experimental analyses considered in this work. Some of them were implemented in CheckMATE-2.0.29 by us. In particular, the validation of the very recent analysis, ATLAS-2106-01676 [90], was presented in Appendix B of this work.

Name	Scenario	Final State	Luminosity(fb ⁻¹)
ATLAS-1909-09226 [86]	$\tilde{\chi}_2^0 \tilde{\chi}_1^\pm \rightarrow W h \tilde{\chi}_1^0 \tilde{\chi}_1^0$	$1\ell + h(h \rightarrow b\bar{b}) + E_T^{\text{miss}}$	139
CMS-SUS-20-001 [91]	$\tilde{\chi}_2^0 \tilde{\chi}_1^\pm \rightarrow W Z \tilde{\chi}_1^0 \tilde{\chi}_1^0$	$2\ell + nj(n>0) + E_T^{\text{miss}}$	137
ATLAS-1912-08479 [84]	$\tilde{\chi}_2^0 \tilde{\chi}_1^\pm \rightarrow W \tilde{\chi}_1^0 Z \tilde{\chi}_1^0$	$3\ell + E_T^{\text{miss}}$	139
ATLAS-1908-08215 [85]	$\tilde{\ell}\tilde{\ell} \rightarrow \ell \tilde{\chi}_1^0 \ell \tilde{\chi}_1^0$ $\tilde{\chi}_1^\pm \tilde{\chi}_1^\mp (\tilde{\chi}_1^\pm \rightarrow \tilde{\ell}\nu/\bar{\nu}\ell)$	$2\ell + E_T^{\text{miss}}$	139
ATLAS-2106-01676 [90]	$\tilde{\chi}_2^0 \tilde{\chi}_1^\pm \rightarrow W^{(*)} Z^{(*)} \tilde{\chi}_1^0 \tilde{\chi}_1^0, W h \tilde{\chi}_1^0 \tilde{\chi}_1^0$	$3\ell + E_T^{\text{miss}}$	139
ATLAS-1803-02762 [171]	$\tilde{\chi}_2^0 \tilde{\chi}_1^\pm \rightarrow W Z \tilde{\chi}_1^0 \tilde{\chi}_1^0, \nu \tilde{\ell} \tilde{\ell}$ $\tilde{\chi}_1^\pm \tilde{\chi}_1^\mp \rightarrow \nu \tilde{\ell} \nu \tilde{\ell}$ $\tilde{\ell}\tilde{\ell} \rightarrow \ell \tilde{\chi}_1^0 \ell \tilde{\chi}_1^0$	$n\ell (n \geq 2) + E_T^{\text{miss}}$	36.1
ATLAS-1802-03158 [172]	$\tilde{g}\tilde{g} \rightarrow 2q \tilde{\chi}_1^0 2q \tilde{\chi}_1^0 (\rightarrow \gamma \tilde{G})$ $\tilde{g}\tilde{g} \rightarrow 2q \tilde{\chi}_1^0 (\rightarrow \gamma \tilde{G}) 2q \tilde{\chi}_1^0 (\rightarrow Z \tilde{G})$ $\tilde{q}\tilde{q} \rightarrow q \tilde{\chi}_1^0 (\rightarrow \gamma \tilde{G}) q \tilde{\chi}_1^0 (\rightarrow \gamma \tilde{G})$ $\tilde{\chi}_2^0 \tilde{\chi}_1^\pm \rightarrow Z/h \tilde{\chi}_1^0 W \tilde{\chi}_1^0$ $\tilde{\chi}_1^\pm \tilde{\chi}_1^\mp \rightarrow W \tilde{\chi}_1^0 W \tilde{\chi}_1^0$	$n\gamma (n \geq 1) + nj(n \geq 0) + E_T^{\text{miss}}$	36.1
ATLAS-1712-08119 [173]	$\tilde{\ell}\tilde{\ell} \rightarrow \ell \tilde{\chi}_1^0 \ell \tilde{\chi}_1^0$ (Wino) $\tilde{\chi}_2^0 \tilde{\chi}_1^\pm \rightarrow W Z \tilde{\chi}_1^0 \tilde{\chi}_1^0$ (Higgsino) $\tilde{\chi}_2^0 \tilde{\chi}_1^\pm + \tilde{\chi}_1^+ \tilde{\chi}_1^- + \tilde{\chi}_2^0 \tilde{\chi}_1^0$	$2\ell + nj(n \geq 0) + E_T^{\text{miss}}$	36.1
CMS-SUS-17-004 [88]	$\tilde{\chi}_2^0 \tilde{\chi}_1^\pm \rightarrow W Z \tilde{\chi}_1^0 \tilde{\chi}_1^0, W H \tilde{\chi}_1^0 \tilde{\chi}_1^0$ $\tilde{\chi}_1^0 \tilde{\chi}_1^0 \rightarrow Z Z \tilde{G}\tilde{G}, H Z \tilde{G}\tilde{G}, H H \tilde{G}\tilde{G}$	$n\ell(n > 0) + E_T^{\text{miss}}$	35.9
CMS-SUS-16-039 [174]	$\tilde{\chi}_2^0 \tilde{\chi}_1^\pm \rightarrow \nu \tilde{\ell} \tilde{\ell}, \nu \tilde{\nu} \tilde{\ell}, \tilde{\tau} \nu \tilde{\ell}, \tilde{\tau} \nu \tilde{\tau}$ $\tilde{\chi}_2^0 \tilde{\chi}_1^\pm \rightarrow W Z \tilde{\chi}_1^0 \tilde{\chi}_1^0, W H \tilde{\chi}_1^0 \tilde{\chi}_1^0$ $\tilde{\chi}_1^0 \tilde{\chi}_1^0 \rightarrow Z Z \tilde{G}\tilde{G}, H Z \tilde{G}\tilde{G}, H H \tilde{G}\tilde{G}$	$n\ell(n > 0) + n\tau(n \geq 0) + E_T^{\text{miss}}$	35.9
CMS-SUS-16-048 [175]	$\tilde{t}\tilde{t} \rightarrow b \tilde{\chi}_1^\pm b \tilde{\chi}_1^\pm$ $\tilde{\chi}_2^0 \tilde{\chi}_1^\pm \rightarrow W^* Z^* \tilde{\chi}_1^0 \tilde{\chi}_1^0$ (Higgsino) $\tilde{\chi}_2^0 \tilde{\chi}_1^\pm / \tilde{\chi}_1^0$	$n\ell(n \geq 0) + nb(n \geq 0) + E_T^{\text{miss}}$	35.9
CMS-SUS-PAS-16-025 [176]	$\tilde{t}\tilde{t} \rightarrow b \tilde{\chi}_1^\pm b \tilde{\chi}_1^\pm$ $\tilde{\chi}_2^0 \tilde{\chi}_1^\pm \rightarrow W^* Z^* \tilde{\chi}_1^0 \tilde{\chi}_1^0$ (Higgsino) $\tilde{\chi}_2^0 \tilde{\chi}_1^\pm / \tilde{\chi}_1^0$	$n\ell(n \geq 0) + nb(n \geq 0) + nj(n \geq 0) + E_T^{\text{miss}}$	12.9
ATLAS-CONF-2016-096 [177]	$\tilde{\chi}_1^\pm \tilde{\chi}_1^\mp (\tilde{\chi}_1^\pm \rightarrow \tilde{\ell}\nu/\bar{\nu}\ell)$ $\tilde{\chi}_1^\pm \tilde{\chi}_2^0 (\tilde{\chi}_1^\pm \rightarrow \tilde{\ell}\nu/\bar{\nu}\ell, \tilde{\chi}_2^0 \rightarrow \tilde{\ell}\ell/\bar{\nu}\nu)$	$n\ell(n \geq 2) + E_T^{\text{miss}}$	13.3

by the package MadGraph_aMC@NLO [167, 168] with the code PYTHIA8 [169] for parton showers, hadronizations, and sparticle decays. The event files were finally input into the package CheckMATE-2.0.29 with the code Delphes [170] for detector simulation.

For each point, 10⁶ MC events were generated in the simulations, and the LHC

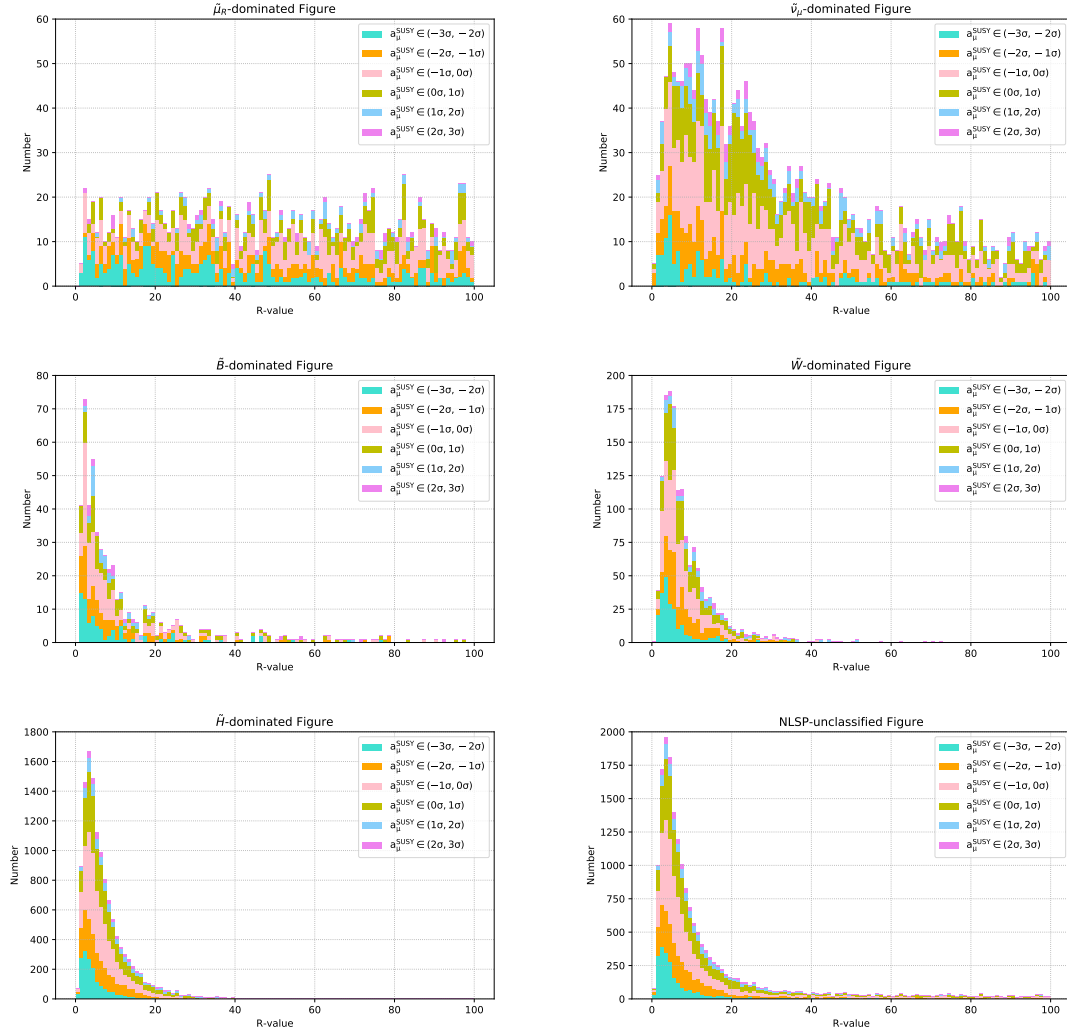


Figure 4. The Histograms of R-value distribution for the different NLSP types. Panels from left to right and top to bottom correspond to the results for the points that NLSP are $\tilde{\mu}_R$, $\tilde{\nu}_\mu$, \tilde{B} -, \tilde{W} -, and \tilde{H} -dominated, respectively. The last panel shows the distribution for all the points. The magnitude of a_μ^{SUSY} is expressed in terms of its deviation from the FNAL measurement center value and is shown by different colors: turquoise for $(-3\sigma, -2\sigma)$, orange for $(-2\sigma, -1\sigma)$, pink for $(-1\sigma, 0\sigma)$, green for $(0\sigma, 1\sigma)$, blue for $(1\sigma, 2\sigma)$, and violet for $(2\sigma, 3\sigma)$.

analyses listed in Table 1 were used to test it. In particular, the following LHC analyses were included in our study, which played a crucial role in constraining the scenario:

1. The search with the ATLAS detector for chargino and slepton pair production with two lepton final states in $\sqrt{s} = 13$ TeV pp collisions (Report No. CERN-EP-2019-106) [85].

2. The search with the ATLAS detector for chargino-neutralino pair production with involved mass splittings near the electroweak scale in three-lepton final states in pp collisions at $\sqrt{s} = 13$ TeV (Report No. CERN-EP-2019-263) [84].
3. The search with the ATLAS detector for the direct production of electroweakinos in final states with one lepton, missing transverse momentum and with a Higgs boson decaying into two b-jets in pp collisions at $\sqrt{s} = 13$ TeV (Report No. CERN-EP-2019-188) [86].
4. The search with the ATLAS detector for chargino-neutralino pair production in final states with three leptons and missing transverse momentum in $\sqrt{s} = 13$ TeV pp collisions (Report No. CERN-EP-2021-059) [90].
5. The combined search with the CMS detector for charginos and neutralinos (Report No. CMS-SUS-17-004) [88].
6. The search with the CMS detector for final states with two oppositely charged same-flavor leptons, jets, and missing transverse momentum in pp collisions at $\sqrt{s} = 13$ TeV (Report No. CMS-SUS-20-001) [91].

The quantity R was used to describe the LHC's limitation on the samples in the discussion. It is defined by $R \equiv \max\{S_i/S_{\text{obs},i}^{95}\}$, where S_i stands for the number of simulated events in the i -th signal region (SR) of all the included analyses, and $S_{\text{obs},i}^{95}$ represents corresponding observed 95% confidence level upper limit. Accordingly, without considering the involved uncertainties, $R > 1$ represents that the considered parameter point is excluded due to the inconsistency with the LHC limit. Otherwise, it is allowed by the LHC searches [108].

The collider simulation results given by **CheckMATE** implied that the LHC searches for SUSY set strong restrictions on the h_2 scenario of the μ NMSSM. In order to display the analysis results clearly, the points were classified by NLSP's dominated component, which may be $\tilde{\mu}_R$, $\tilde{\nu}_\mu$, \tilde{B} , \tilde{W} , or \tilde{H} . The Histograms of R-value distribution for the different NLSP types were displayed in Fig. 4 from left to right and top to bottom, respectively. Points colored by turquoise, orange, pink, green, blue, and violet correspond respectively to the cases that a_μ^{SUSY} are in the range of $(-3\sigma, -2\sigma)$, $(-2\sigma, -1\sigma)$, $(-1\sigma, 0\sigma)$, $(0\sigma, 1\sigma)$, $(1\sigma, 2\sigma)$ and $(2\sigma, 3\sigma)$. The results were also summarized in Table 2, which includes the number of samples obtained by the scan (denoted N_{tot}), that satisfying $R < 1$ (denoted by N_{pass}), and the more detailed classification of N_{tot} and N_{pass} by the ranges of a_μ^{SUSY} .

According to Table 2 and Figs. 4, the following conclusions are inferred:

- Among the five types of NLSP, the \tilde{H} -dominated NLSP is the easiest one for explaining the discrepancy in the h_2 scenario, and by contrast, the \tilde{B} -dominated NLSP is the least preferred one (see N_{tot} in Table 2). The LHC restrictions are

NLSP	\tilde{H}	\tilde{B}	\tilde{W}	$\tilde{\mu}_R$	$\tilde{\nu}_\mu$
$N_{\text{tot}} \mid N_{\text{pass}}$	15356 221	756 12	3116 4	3304 2	3408 9
$N_{a_\mu^{\text{SUSY}}} \in (-3\sigma, -2\sigma)$	1728 33	92 0	364 1	406 0	271 3
$N_{a_\mu^{\text{SUSY}}} \in (-2\sigma, -1\sigma)$	2370 17	126 0	518 0	527 0	449 2
$N_{a_\mu^{\text{SUSY}}} \in (-1\sigma, 0\sigma)$	4380 15	196 0	926 0	899 0	1059 1
$N_{a_\mu^{\text{SUSY}}} \in (0\sigma, 1\sigma)$	3497 6	135 0	721 0	632 0	851 1
$N_{a_\mu^{\text{SUSY}}} \in (1\sigma, 2\sigma)$	982 0	48 0	200 0	216 0	242 0
$N_{a_\mu^{\text{SUSY}}} \in (2\sigma, 3\sigma)$	462 0	21 0	79 0	100 0	122 0

Table 2. Numbers of the samples classified by NLSP’s dominant component. N_{tot} denotes the total number for each type samples, which were obtained by the scan and sequently surveyed by MC simulations, N_{pass} represents the number of the points satisfying $R < 1$, and $N_{a_\mu^{\text{SUSY}}}$ corresponds to further classifications of N_{tot} and N_{pass} by the magnitude of a_μ^{SUSY} . It was verified that the R -values were always larger than 0.4, which means that all the samples are to be tested at high-luminosity LHC, and that all samples passing the LHC constraints were characterized by $|m_{\tilde{\chi}_1^0}| > 110$ GeV.

extremely strong in excluding parameter points for any type of NLSP (see N_{pass} in the table). In particular, they are strengthened significantly once the scenario is required to explain the discrepancy at 3σ level (see $N_{a_\mu^{\text{SUSY}}}$ in the table). Specifically, it takes dozens of parameter points with \tilde{H} -dominated NLSP and only few points with $\tilde{\nu}_\mu$ -dominated NLSP to interpret the discrepancy at the 3σ level. This situation reflects the difficulty of the h_2 scenario in explaining the discrepancy. One fundamental reason comes from the fact that the scenario prefers a relatively small $\tan\beta$ and μ_{tot} , and hence moderately light sparticles are predicted to obtain a sizable a_μ^{SUSY} .

It was verified that, among the experimental analyses, the analysis 4 usually sets the tightest constraints. In the case that the parameter points predict sizable signals with four or more leptons, analysis 5 could also impose the strongest restriction.

- In the case of $\tilde{\mu}_R$ - or $\tilde{\nu}_\mu$ -dominated NLSP, Wino- and Higgsino-dominated electroweakinos will decay mainly into leptonic final states via slepton and/or sneutrino, which proliferates the lepton signals. As a result, R can reach 100 for lots of points, which is shown on the top left and right panels in Fig. 4. In addition, the LHC constraints on the $\tilde{\mu}_R$ -dominated NLSP point are usually tighter than those on the $\tilde{\nu}_\mu$ -dominated NLSP point because neutralinos will decay by $\tilde{\chi}_i^0 \rightarrow \tilde{\mu}^\pm \mu^\mp \rightarrow \tilde{\chi}_1^0 \mu^+ \mu^-$ for the former case and by $\tilde{\chi}_i^0 \rightarrow \tilde{\mu}^\pm \mu^\mp, \tilde{\nu}_\mu \nu \rightarrow \tilde{\chi}_1^0 \mu^+ \mu^-, \tilde{\chi}_1^0 \nu \nu$ for the latter case. The former case can produce more μ leptons.

- In the case of \tilde{B} -dominated NLSP, although most parameter points correspond to $R < 20$, there are still a few points that predict $R > 80$. It was verified that the dominant decays of $\tilde{\chi}_2^0$ include $\tilde{\chi}_2^0 \rightarrow \tilde{\chi}_1^0 Z^{(*)}$, $\tilde{\chi}_1^0 h_{1,2}$, $\tilde{\chi}_1^0 \mu^+ \mu^-$, and smuons decay mainly by $\tilde{\mu}_{1,2} \rightarrow \mu \tilde{\chi}_2^0$ for most points. If the kinetics is allowed, other heavy sparticles prefer to decay dominantly into $\tilde{\chi}_2^0$ since they couple to $\tilde{\chi}_2^0$ by non-suppressed gauge couplings. For points with $R > 50$, $\tilde{\chi}_2^0 \rightarrow \tilde{\chi}_1^0 \mu^+ \mu^-$ is usually the largest decay channel of $\tilde{\chi}_2^0$, and the strongest constraints come from the analysis of four or more lepton signals in analysis 5.
- In the case of \tilde{W} -dominated NLSP, most points predict $R < 20$, but in very rare case R may reach 70. Detailed study indicated that $\tilde{\chi}_2^0$ decays mainly by $\tilde{\chi}_2^0 \rightarrow \tilde{\chi}_1^0 Z^{(*)}$, $\tilde{\chi}_1^0 h_{1,2}$ for most points, and $\tilde{\chi}_2^0 \rightarrow \tilde{\chi}_1^0 \mu^+ \mu^-$, $\tilde{\chi}_1^0 \nu \nu$ are the dominant decay only for a small portion of the points. It also indicated that $\tilde{\chi}_1^\pm$ decays mainly by $\tilde{\chi}_1^\pm \rightarrow \tilde{\chi}_1^0 W^{(*)}$ for nearly all points, and smuons decay in a complex way, e.g., any of the channels $\tilde{\mu} \rightarrow \tilde{\chi}_i^0 \mu$ ($i = 1, \dots, 5$), $\tilde{\chi}_{1,2}^- \nu$ may be the dominant decay.

It is notable that R in the \tilde{W} -dominated NLSP case can not be exceedingly large. This conclusion comes from the fact that the \tilde{W} -dominated electroweakinos are forbidden to decay into sleptons directly, and thus, even in the optimum case, the lepton signal from the decay $\tilde{\chi}_2^0 \rightarrow \tilde{\mu}^{\pm*} \mu^\mp \rightarrow \tilde{\chi}_1^0 \mu^+ \mu^-$ is not much larger than the other final states. Consequently, $pp \rightarrow \tilde{\chi}_2^0 \tilde{\chi}_1^\pm$, which is the largest sparticle production process, can not generate tri-lepton signal events efficiently. This feature results in a smaller signal rate than the \tilde{B} -dominated NLSP case, where the Wino-dominated electroweakinos may decay far dominantly into leptons.

- By considering the \tilde{H} -dominated NLSP case it was found that the decay modes of $\tilde{\chi}_2^0$, $\tilde{\chi}_1^\pm$ and $\tilde{\mu}_{1,2}$ are similar to those of the \tilde{W} -dominated NLSP case, and the LHC constraints tend to be weaker than the other cases. This observation may be understood from four aspects [67]. First, since the \tilde{H} -dominated $\tilde{\chi}_{2,3}^0$ and $\tilde{\chi}_1^\pm$ can not decay into sleptons, the leptonic signal rate is usually much smaller than the case where $\tilde{\mu}_R$ or $\tilde{\nu}_\mu$ acts as NLSP. Second, the collider sensitive signal events are often diluted by the complicated decay chains of sparticles, given that heavy sparticles prefer to decay into the NLSP or other non-singlet-dominated sparticles first. They are diluted also by the decays $\tilde{\chi}_{2,3}^0 \rightarrow \tilde{\chi}_1^0 h_s$, $\tilde{\chi}_1^0 h$, given that $Br(h_s/h \rightarrow \ell^\pm \ell^\mp)$ is much smaller than $Br(Z \rightarrow \ell^\pm \ell^\mp)$. Third, the interpretation of Δa_μ requires that all crucial sparticles are usually in several hundred GeVs for a not too large $\tan \beta$. Thus, for the parameter points surviving the LHC constraints, the mass splitting between sparticles is not large enough to produce high- p_T signal objects, which can be significantly distinguished from the background in the collider. Last, in some rare cases, the leptonic signal

Table 3. Detailed information of two benchmark points consistent with the DM and Higgs experiments. The point P1 is allowed by the LHC search for SUSY, while the point P2 has been excluded. Both of them predict $a_\mu^{\text{SUSY}} \simeq 2.51 \times 10^{-9}$.

Benchmark Point P1			Benchmark Point P2				
λ	0.059	m_{h_u}	30.4 GeV	λ	0.094	m_{h_u}	91.0 GeV
κ	-0.12	m_{A_u}	209.3 GeV	κ	-0.17	m_{A_u}	180.2 GeV
$\tan\beta$	24.99	m_h	124.7 GeV	$\tan\beta$	12.75	m_h	124.8 GeV
μ	170.5 GeV	m_H	1053 GeV	μ	157.6 GeV	m_H	1023 GeV
$\mu + \mu_{\text{eff}}$	200.5 GeV	m_{A_H}	1052 GeV	$\mu + \mu_{\text{eff}}$	195.7 GeV	m_{A_H}	1023 GeV
A_t	-2284 GeV	$m_{\tilde{\chi}_1^0}$	-126.6 GeV	A_t	2078 GeV	$m_{\tilde{\chi}_1^0}$	-136.5 GeV
A_κ	231.6 GeV	$m_{\tilde{\chi}_2^0}$	194.6 GeV	A_κ	158.4 GeV	$m_{\tilde{\chi}_2^0}$	156.6 GeV
M_1	-767.1 GeV	$m_{\tilde{\chi}_3^0}$	-210.0 GeV	M_1	957.8 GeV	$m_{\tilde{\chi}_3^0}$	-209.6 GeV
M_2	429.0 GeV	$m_{\tilde{\chi}_4^0}$	468.1 GeV	M_2	217.8 GeV	$m_{\tilde{\chi}_4^0}$	281.1 GeV
m_L	524.7 GeV	$m_{\tilde{\chi}_5^0}$	-770.6 GeV	m_L	322.6 GeV	$m_{\tilde{\chi}_5^0}$	961.1 GeV
m_E	525.9 GeV	$m_{\tilde{\chi}_1^\pm}$	198.1 GeV	m_E	306.6 GeV	$m_{\tilde{\chi}_1^\pm}$	160.6 GeV
σ_μ^{SUSY}	1.99×10^{-9}	$m_{\tilde{\chi}_2^\pm}$	468.6 GeV	σ_μ^{SUSY}	2.51×10^{-9}	$m_{\tilde{\chi}_2^\pm}$	284.6 GeV
Ωh^2	0.085	$m_{\tilde{\mu}_L}$	531.4 GeV	Ωh^2	0.099	$m_{\tilde{\mu}_L}$	329.1 GeV
σ_p^{SI}	$1.40 \times 10^{-47} \text{cm}^2$	$m_{\tilde{\mu}_R}$	532.7 GeV	σ_p^{SI}	$4.93 \times 10^{-47} \text{cm}^2$	$m_{\tilde{\mu}_R}$	493.8 GeV
σ_n^{SD}	$4.30 \times 10^{-42} \text{cm}^2$	$m_{\tilde{\nu}_\mu}$	525.5 GeV	σ_n^{SD}	$4.41 \times 10^{-43} \text{cm}^2$	$m_{\tilde{\nu}_\mu}$	319.0 GeV
$N_{11}, N_{12}, N_{13}, N_{14}, N_{15}$	0.005, 0.010, 0.046, 0.077, -0.996			$N_{11}, N_{12}, N_{13}, N_{14}, N_{15}$	-0.005, 0.029, 0.09, 0.141, -0.986		
$N_{21}, N_{22}, N_{23}, N_{24}, N_{25}$	-0.032, -0.216, 0.709, -0.670, -0.021			$N_{21}, N_{22}, N_{23}, N_{24}, N_{25}$	0.03, -0.586, 0.631, -0.506, -0.032		
$N_{31}, N_{32}, N_{33}, N_{34}, N_{35}$	0.053, 0.082, 0.697, 0.705, 0.088			$N_{31}, N_{32}, N_{33}, N_{34}, N_{35}$	-0.024, 0.117, 0.682, 0.702, 0.166		
$N_{41}, N_{42}, N_{43}, N_{44}, N_{45}$	-0.008, 0.973, 0.098, -0.209, -0.002			$N_{41}, N_{42}, N_{43}, N_{44}, N_{45}$	0.033, 0.801, 0.359, -0.478, -0.012		
$N_{51}, N_{52}, N_{53}, N_{54}, N_{55}$	0.998, -0.004, -0.014, -0.06, -4.7E-05			$N_{51}, N_{52}, N_{53}, N_{54}, N_{55}$	0.999, -0.005, -0.014, 0.049, -1.63E-05		
Annihilations	Fractions[%]			Annihilations	Fractions[%]		
$\tilde{\chi}_1^0 \tilde{\chi}_1^0 \rightarrow h_u A_u / h_u h_u$	98.1/1.3			$\tilde{\chi}_1^0 \tilde{\chi}_1^0 \rightarrow h_u A_u / h_u h_u$	86.0/4.5		
Decays	Branching ratios[%]			Decays	Branching ratios[%]		
$\tilde{\chi}_2^0 \rightarrow \tilde{\chi}_1^0 Z^*$	100			$\tilde{\chi}_2^0 \rightarrow \tilde{\chi}_1^0 Z^*$	100		
$\tilde{\chi}_3^0 \rightarrow \tilde{\chi}_1^0 h_u / \tilde{\chi}_1^0 Z^*$	95.8/3.9			$\tilde{\chi}_3^0 \rightarrow \tilde{\chi}_1^\mp W^+ / \tilde{\chi}_3^0 Z^* / \tilde{\chi}_1^0 Z^*$	64.0/34.1/1.9		
$\tilde{\chi}_4^0 \rightarrow \tilde{\chi}_1^\mp W^\mp / \tilde{\chi}_3^0 Z / \tilde{\chi}_2^0 h / \tilde{\chi}_2^0 Z / \tilde{\chi}_3^0 h$	56.7/20.5/16.8/1.9			$\tilde{\chi}_4^0 \rightarrow \tilde{\chi}_1^\mp W^\mp / \tilde{\chi}_1^0 Z$	96.8/2.4		
$\tilde{\chi}_5^0 \rightarrow \tilde{\chi}_1^\mp W^\mp / \tilde{\nu}_\mu \nu_\mu / \tilde{\mu}_L^\pm \mu^\mp / \tilde{\chi}_3^0 Z / \tilde{\chi}_2^0 h / \tilde{\chi}_2^0 Z / \tilde{\chi}_3^0 h$	24.8/23.7/19.1/12.3/10/3.6/2.0			$\tilde{\chi}_5^0 \rightarrow \tilde{\mu}_R^\pm \mu^\mp / \tilde{\nu}_\mu \nu_\mu / \tilde{\mu}_L^\pm \mu^\mp / \tilde{\chi}_2^\mp W^\mp / \tilde{\chi}_1^\mp W^\mp / \tilde{\chi}_3^0 Z / \tilde{\chi}_4^0 h / \tilde{\chi}_2^0 h / \tilde{\chi}_3^0 h$	46.6/11.9/11.3/9.0/5.7/5.5/3.5/2.4/1.6		
$\tilde{\chi}_1^\pm \rightarrow \tilde{\chi}_1^0 W^*$	100			$\tilde{\chi}_1^\pm \rightarrow \tilde{\chi}_1^0 W^* / \tilde{\chi}_3^0 W^*$	99.1/0.9		
$\tilde{\chi}_2^\pm \rightarrow \tilde{\chi}_3^0 W^\pm / \tilde{\chi}_3^0 W^\pm / \tilde{\chi}_1^\pm Z / \tilde{\chi}_1^\pm h$	26.7/26.4/25.6/20.5			$\tilde{\chi}_2^\pm \rightarrow \tilde{\chi}_3^0 W^\pm / \tilde{\chi}_1^\mp Z / \tilde{\chi}_1^0 W^\pm$	57.5/36.2/5.2		
$\tilde{\mu}_L^\pm \rightarrow \tilde{\chi}_2^\pm \nu_\mu / \tilde{\chi}_3^0 \mu^\pm / \tilde{\chi}_2^0 \mu^\pm / \tilde{\chi}_3^0 \mu^\pm / \tilde{\chi}_1^\pm \nu_\mu$	41.5/20.1/14.9/3.9			$\tilde{\mu}_L^\pm \rightarrow \tilde{\chi}_1^\pm \nu_\mu / \tilde{\chi}_2^0 \mu^\pm / \tilde{\chi}_2^\pm \nu_\mu / \tilde{\chi}_3^0 \mu^\pm$	47.8/29.7/14.2/4.5		
$\tilde{\nu}_\mu \rightarrow \tilde{\chi}_2^\pm \nu_\mu / \tilde{\chi}_3^0 \mu^\pm / \tilde{\chi}_2^0 \mu^\pm / \tilde{\chi}_3^0 \mu^\pm / \tilde{\chi}_1^\pm \nu_\mu$	46.0/22.3/10.8/5.9			$\tilde{\nu}_\mu \rightarrow \tilde{\chi}_2^\pm \mu^\mp / \tilde{\chi}_1^\pm \nu_\mu / \tilde{\chi}_3^0 \mu^\mp / \tilde{\chi}_4^0 \mu^\pm / \tilde{\chi}_2^\pm \nu_\mu$	48.0/36.2/9.6/3.4/1.8		
$\tilde{\nu}_\mu \rightarrow \tilde{\chi}_1^\mp \mu^\mp / \tilde{\chi}_2^\mp \mu^\mp / \tilde{\chi}_3^0 \nu_\mu / \tilde{\chi}_3^0 \nu_\mu$	47.2/27.2/14.5/10.4			$\tilde{\nu}_\mu \rightarrow \tilde{\chi}_1^\mp \mu^\mp / \tilde{\chi}_2^\mp \nu_\mu / \tilde{\chi}_3^0 \mu^\mp / \tilde{\chi}_4^0 \nu_\mu$	65.7/24.9/5.0/3.6		
R value	0.84			R value	4.14		

of SUSY may mainly come from the NLSP. For this situation, the discussion of the LHC constraints can be simplified by considering the system that only contains NLSP and LSP. From this, it is evident that the constraints on the \tilde{H} -dominated NLSP case are significantly weaker than those on the \tilde{W} -dominated NLSP case. In fact, we once scrutinized the property of all the samples surviving the LHC constraints. It was found that the above factors applied to these samples.

In order to emphasize the characteristics of the parameter point with \tilde{H} -dominated NLSP, two benchmark points, P1 and P2, are chosen to present their detailed information in Table 3. Both points satisfy the DM constraints and can explain the a_μ discrepancy at 2σ level. The P1 point survives the LHC constraints, while the P2 point has been excluded by the LHC search for SUSY. These two benchmark points verify part of the discussions in this work.

Finally, it should be noted that the LHC search for τ -leptons plus missing momentum signal, such as the ATLAS analyses in [178] and [179], was not considered because of the massive $\tilde{\tau}$ assumption in this study. Specifically, the assumption implies that the τ -leptons mainly come from the decay of the W/Z or Higgs bosons, which are the decay products of parent sparticles. For the former case, the final

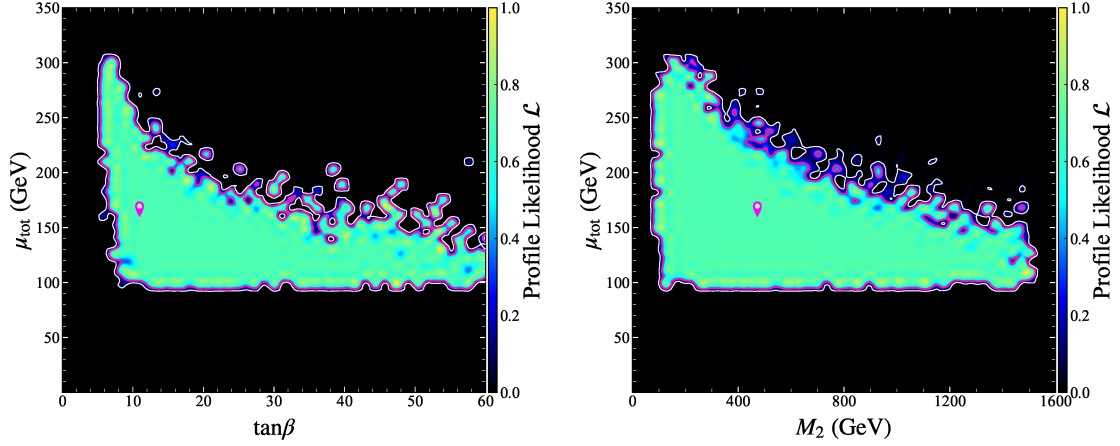


Figure 5. Same as Fig. 1, but for the results of the GNMSSM. The best point is located at $\tan\beta \simeq 10.9$, $m_{\tilde{\chi}_1^0} \simeq 42.8$ GeV, $\mu_{tot} \simeq 160$ GeV, $M_2 \simeq 473$ GeV, $m_{\tilde{\mu}_L} \simeq 164$ GeV, and $m_{\tilde{\mu}_R} \simeq 143$ GeV.

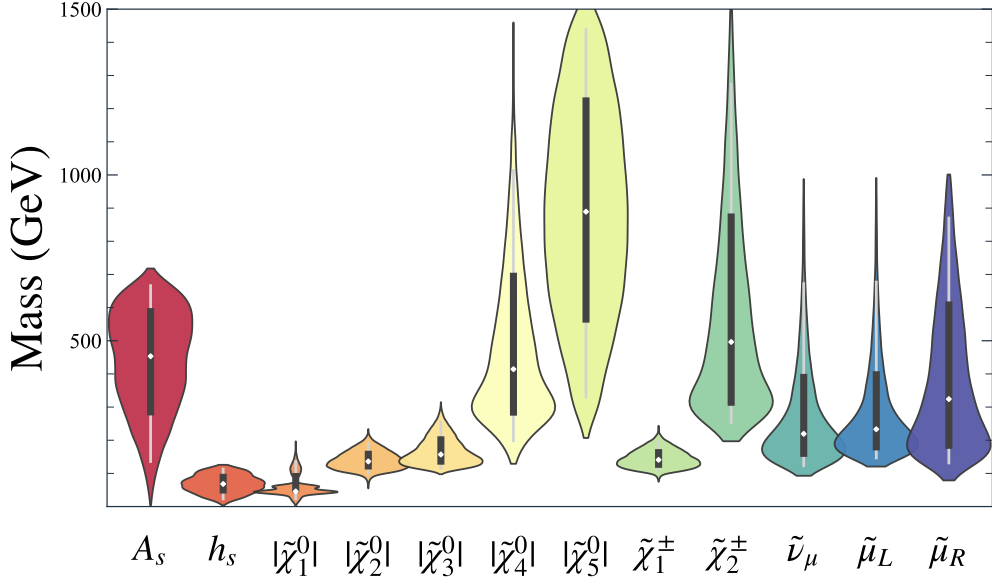


Figure 6. Same as Fig. 3, but for the results of the GNMSSM.

states containing e and/or μ are more efficient than the τ final state in restricting SUSY mass spectrum since all the lepton signal rates are roughly equal. For the latter case, the τ signal is usually less crucial in SUSY search because the branching ratio of the Higgs decay into $\tau\bar{\tau}$ is significantly small (in comparison with $\tilde{\tau}$ decay). With the codes for the analyses in [178] and [179], which were implemented in our previous work [164] and CheckMATE-2.0.29, respectively, we studied their prediction of R for the two benchmark points. We found that the analyses do not affect the results in Table 3. As an alternative, if $\tilde{\tau}$ or all sleptons are assumed to the NLSP

NLSP	\tilde{H}	\tilde{B}	\tilde{W}	$\tilde{\mu}_R$	$\tilde{\nu}_\mu$
$N_{\text{tot}} \mid N_{\text{pass}}$	11753 21	470 0	1259 0	867 0	2041 0
$N_{a_\mu^{\text{SUSY}}} \in (-3\sigma, -2\sigma)$	1519 5	67 0	105 0	92 0	104 0
$N_{a_\mu^{\text{SUSY}}} \in (-2\sigma, -1\sigma)$	2113 3	97 0	180 0	154 0	270 0
$N_{a_\mu^{\text{SUSY}}} \in (-1\sigma, 0\sigma)$	3777 1	137 0	448 0	314 0	906 0
$N_{a_\mu^{\text{SUSY}}} \in (0\sigma, 1\sigma)$	2462 0	83 0	361 0	180 0	578 0
$N_{a_\mu^{\text{SUSY}}} \in (1\sigma, 2\sigma)$	499 0	27 0	65 0	26 0	117 0
$N_{a_\mu^{\text{SUSY}}} \in (2\sigma, 3\sigma)$	224 0	14 0	19 0	35 0	14 0

Table 4. Same as Table 2, but for the results of the GNMSSM. All samples predict $R > 0.4$, thus they are to be tested at high-luminosity LHC. Moreover, all samples passing the LHC constraints are characterized by $|m_{\tilde{\chi}_1^0}| \gtrsim 150$ GeV.

(see, e.g., [41]), the production rate of the e/μ final states will be affected. In this case, R should be recalculated. In particular, the experimental analysis of the τ final state must be included in the study. It is expected that the LHC constraints are still strong because the h_2 scenario is featured by moderately light Higgsinos.

4 Explaining Δa_μ in the h_2 scenario of GNMSSM

The impact of the muon $g-2$ anomaly on the h_2 scenario of the GNMSSM is studied in this section. For this purpose, the parameter space including $|\mu'| \leq 1$ TeV, $-10^6 \text{ TeV}^2 \leq m_S'^2 \leq 10^6 \text{ TeV}^2$, and that in Eq. (3.1), were scanned in a way similar to what we did in Section 3. It was found that the DM was Singlino-dominated for all the obtained samples, and it annihilated mainly by a resonant Z , h , or h_s/A_s to obtain the measured abundance. These channels contributed to the total Bayesian evidence by about 43%, 19.6%, and 37%, respectively, before the MC simulations were implemented. The basic reason for such a behavior is that $\tilde{\chi}_1^0$, m_{h_s} and m_{A_s} in the GNMSSM can be changed freely by tuning μ' , A_κ , and $m_S'^2$, respectively. Thus, the annihilations could easily happen. Given that the GNMSSM might have different key features from the μ NMSSM, various PL maps of the GNMSSM were surveyed in this study.

In Fig. 5, the two-dimensional profile likelihood function was projected onto $\tan \beta - \mu_{\text{tot}}$ and $M_2 - \mu_{\text{tot}}$ planes. They show that the GNMSSM results are quite similar to the μ NMSSM predictions. In particular, μ_{tot} and $m_{\tilde{\chi}_1^\pm}$ have upper bounds of about 310 GeV and 300 GeV, respectively⁹. The fundamental reason for this, as was emphasized before, is that the h_2 scenario prefers moderately small μ_{tot} and

⁹We inferred that the 2σ CI of the μ NMSSM covers a broader region on the parameter planes than that of the GNMSSM by comparing Fig. 5 with Fig. 1. This is contrary to the common sense that the former should be narrower than the latter since the parameter space of the μ NMSSM is only a subset of the GNMSSM's parameter space. This phenomenon originates from the MultiNest

$\tan\beta$ to predict $m_{h_1} \lesssim 125$ GeV and h_2 to be SM-like, which was verified by the posterior probability distribution function of the samples obtained from the scan. This characteristic, once combined with the requirement to explain the anomaly, will entail certain moderately light sparticles. In Fig. 6, the violin diagrams for the mass spectrum of the singlet-dominated Higgs bosons, the electroweakinos and μ -type sleptons are shown. The profiles for the sparticles are quite similar to those in Fig. 3 for the μ NMSSM results, except that $|m_{\tilde{\chi}_1^0}|$ can be as low as several GeV. This difference mainly comes from the DM annihilation mechanisms, and it usually makes the LHC's constraints much stronger.

In Table 4, the numbers of the samples surveyed by MC simulations and those passing the LHC constraints were presented in a way similar to Table 2. This table shows that the LHC analyses have strongly constrained the parameter space of the GNMSSM.

5 Conclusion

The recent measurement of a_μ by the FNAL corroborates further the long-standing discrepancy of a_μ^{Exp} from a_μ^{SM} . It can not only reveal useful information of the physics beyond the SM, but also place strong restrictions on certain theories. Recently, implications of the discrepancy were comprehensively discussed with respect to the GNMSSM, which is a theory that has the following attractive features: it is free from the tadpole problem and the domain-wall problem of the Z_3 -NMSSM, and it is capable of forming an economic secluded DM sector to naturally yield the DM experimental results [116]. It was found that the h_1 scenario of the GNMSSM could easily and significantly weaken the constraints from the LHC search for SUSY. It also predicted more stable vacuums than the Z_3 -NMSSM. As a result, the scenario can explain the discrepancy in a broad parameter space that is consistent with all experimental results, and at same time keeps the electroweak symmetry breaking natural [67]. By contrast, it is difficult for the popular MSSM and Z_3 -NMSSM to do this.

These theoretical advantages inspired us to consider the h_2 scenario of the GNMSSM, which is another well-known realization of the theory. It was shown by analytic formulae that, in order to obtain $m_{h_1} \lesssim 125$ GeV and an SM-like h_2 without significant tunings of relevant parameters, the scenario prefers a moderately light μ_{tot}

algorithm utilized in the scan, which mainly collects the samples contributing significantly to the Bayesian evidence [135]. The parameter points of the μ NMSSM correspond to $\mu' = 0$ and $m_S'^2 = 0$, and are relatively unimportant for the evidence, which was verified by the study of the two-dimensional posterior probability distribution function, $P(\mu', m_S'^2)$ [163]. Thus, only a few of them were considered in the sampling. It is expected that, with the increase of the setting n_{live} , more samples of the GNMSSM will be collected, which will broaden the CI regions [164]. This process, however, is very computationally expensive, since a high-dimensional parameter space is surveyed.

and $\tan\beta \lesssim 30$. This characteristic, if combined with the requirement to account for the anomaly, will entail some light sparticles, and sequentially make the LHC constraints rather tight. In this work, this speculation was tested using numerical results. Specifically, a special case of the GNMSSM called μ NMSSM was first studied by scanning its parameter space with the MultiNest algorithm and considering the constraints from the LHC Higgs data, the DM experimental results, the B-physics observations, and the vacuum stability. Then, the samples obtained from the scan were surveyed by the LHC analyses in sparticle searches. Through sophisticated MC simulations, it was found that only a dozen of the samples, among about twenty thousand, passed the constraints, which corresponded to about 0.04% of the total Bayesian evidence. Given that the scan results have statistical significance, we conclude that the h_2 scenario of the μ NMSSM is tightly constrained if it is intended to explain the anomaly. A similar study was carried out for the GNMSSM, and it was found that a smaller portion of the samples (about 0.008% of the total evidence) satisfied the LHC constraints. This difference arises from DM annihilation mechanisms: for the former case, the Singlino-dominated DM achieved the measured abundance mainly through the process $\tilde{\chi}_1^0 \tilde{\chi}_1^0 \rightarrow h_s A_s$, while for the latter case, it was through a resonant Z , h , or h_s/A_s annihilation to obtain the abundance. Since the latter case usually predicts a relatively light DM, the LHC constraints are stronger.

This work extends the research in [99] by considering a more general theoretical framework with more advanced and sophisticated research strategies. As a result, the conclusions obtained in this work are more robust than those of the previous work, and apply to any realizations of the NMSSM.

Acknowledgement

J. Cao and Y. Yue thank Dr. H. J. Zhou for her great patience in reading the manuscript carefully and giving good suggestions. This work is supported by the National Natural Science Foundation of China (NNSFC) under grant No. 12075076.

A DM-nucleon scattering in the MSSM

In this section, we use analytic formulae to focus on Bino-dominated DM and study DM-nucleon scatterings for three typical cases.

We begin with the neutralino mass matrix given by [180]:

$$M_N = \begin{pmatrix} M_1 & 0 & -\frac{vg_1 c_\beta}{2} & \frac{vg_1 s_\beta}{2} \\ 0 & M_2 & \frac{vc_W g_1 c_\beta}{2s_W} & -\frac{vc_W g_1 s_\beta}{2s_W} \\ -\frac{vg_1 c_\beta}{2} & \frac{vc_W g_1 c_\beta}{2s_W} & 0 & -\mu \\ \frac{vg_1 s_\beta}{2} & -\frac{vc_W g_1 s_\beta}{2s_W} & -\mu & 0 \end{pmatrix}, \quad (\text{A.1})$$

where $g_1 = 2M_Z s_W/v$, $s_\beta \equiv \sin \beta$ and $c_\beta \equiv \cos \beta$. In terms of neutralino mass, $m_{\tilde{\chi}_i^0}$, the eigenvectors are then exactly formulated by

$$N_i = \frac{1}{\sqrt{C_i}} \begin{pmatrix} \left(\mu^2 - m_{\tilde{\chi}_i^0}^2 \right) \left(M_2 - m_{\tilde{\chi}_i^0} \right) - M_Z^2 c_W^2 \left(m_{\tilde{\chi}_i^0} + 2\mu s_\beta c_\beta \right) \\ -M_Z^2 s_W c_W \left(m_{\tilde{\chi}_i^0} + 2\mu s_\beta c_\beta \right) \\ \left(M_2 - m_{\tilde{\chi}_i^0} \right) \left(m_{\tilde{\chi}_i^0} c_\beta + \mu s_\beta \right) M_Z s_W \\ - \left(M_2 - m_{\tilde{\chi}_i^0} \right) \left(m_{\tilde{\chi}_i^0} s_\beta + \mu c_\beta \right) M_Z s_W \end{pmatrix}$$

where

$$C_i = M_Z^2 c_W^2 \left(m_{\tilde{\chi}_i^0} + 2\mu s_\beta c_\beta \right) \left[M_Z^2 \left(m_{\tilde{\chi}_i^0} + 2\mu s_\beta c_\beta \right) + 2 \left(\mu^2 - m_{\tilde{\chi}_i^0}^2 \right) \left(m_{\tilde{\chi}_i^0} - M_2 \right) \right] \\ + \left(m_{\tilde{\chi}_i^0} - M_2 \right)^2 \left\{ M_Z^2 s_W^2 \left[\left(m_{\tilde{\chi}_i^0}^2 + \mu^2 \right) + 4\mu m_{\tilde{\chi}_i^0} s_\beta c_\beta \right] + \left(m_{\tilde{\chi}_i^0}^2 - \mu^2 \right)^2 \right\}.$$

Parameterizing the couplings of the DM to the SM-like Higgs boson, h , and Z boson as the following form [26, 93]

$$\mathcal{L}_{\text{MSSM}} \ni C_{\tilde{\chi}_1^0 \tilde{\chi}_1^0 h} h \tilde{\chi}_1^0 \tilde{\chi}_1^0 + C_{\tilde{\chi}_1^0 \tilde{\chi}_1^0 Z} Z_\mu \tilde{\chi}_1^0 \gamma^\mu \gamma_5 \tilde{\chi}_1^0,$$

we obtain [112]

$$C_{\tilde{\chi}_1^0 \tilde{\chi}_1^0 h} = \frac{e \tan \theta_w}{C_1} \left(\mu^2 - m_{\tilde{\chi}_1^0}^2 \right) \left(M_2 - m_{\tilde{\chi}_1^0} \right)^2 M_Z \left[m_{\tilde{\chi}_1^0} \sin(\beta - \alpha) + \mu \cos(\beta + \alpha) \right], \\ C_{\tilde{\chi}_1^0 \tilde{\chi}_1^0 Z} = \frac{e \tan \theta_w \cos 2\beta}{2C_1} \left(\mu^2 - m_{\tilde{\chi}_1^0}^2 \right) \left(M_2 - m_{\tilde{\chi}_1^0} \right)^2 M_Z^2, \quad (\text{A.2})$$

where α is the mixing angle of CP-even Higgs fields in forming mass eigenstates [94]. In the decoupling limit of the Higgs sector, i.e., $m_A \gg v$, the SI and SD cross-sections of the DM with nucleons are approximated by [112]:

$$\sigma_{\tilde{\chi}_1^0-N}^{\text{SI}} \simeq 5 \times 10^{-45} \text{cm}^2 \left(\frac{C_{\tilde{\chi}_1^0 \tilde{\chi}_1^0 h}}{0.1} \right)^2 \left(\frac{m_h}{125 \text{GeV}} \right)^2, \quad (\text{A.3})$$

$$\sigma_{\tilde{\chi}_1^0-N}^{\text{SD}} \simeq C_N \times \left(\frac{C_{\tilde{\chi}_1^0 \tilde{\chi}_1^0 Z}}{0.01} \right)^2, \quad (\text{A.4})$$

with $C_p \simeq 2.9 \times 10^{-41} \text{cm}^2$ for protons and $C_n \simeq 2.3 \times 10^{-41} \text{cm}^2$ for neutrons.

In the following, we assume $\tan \beta \gg 1$ and $m_A \gg v$ so that $\alpha \simeq \beta - \pi/2$ [94], and investigate the dependence of $\sigma_{\tilde{\chi}_1^0-N}^{\text{SI}}$ and $\sigma_{\tilde{\chi}_1^0-N}^{\text{SD}}$ on parameter μ for three cases.

- Case I: the DM co-annihilated with the Wino-dominated electroweakinos to obtain the measured abundance, M_2 and $m_{\tilde{\chi}_1^0}$ are of same sign, and $|\mu|$ is comparable with $|m_{\tilde{\chi}_1^0}|$. In this case, $M_2 \simeq 1.1 \times m_{\tilde{\chi}_1^0}$ to obtain the measured DM abundance, and C_1 is approximated by:

$$C_1 \simeq M_Z^4 c_w^2 \left(m_{\tilde{\chi}_1^0} + \mu \sin 2\beta \right)^2 \simeq M_Z^4 c_w^2 m_{\tilde{\chi}_1^0}^2. \quad (\text{A.5})$$

Consequently, $C_{h\tilde{\chi}_1^0\tilde{\chi}_1^0}$ and $C_{Z\tilde{\chi}_1^0\tilde{\chi}_1^0}$ are given by:

$$\begin{aligned} C_{\tilde{\chi}_1^0\tilde{\chi}_1^0 h} &\simeq 0.01 \times e \tan \theta_w \frac{m_{\tilde{\chi}_1^0} \left(\mu^2 - m_{\tilde{\chi}_1^0}^2 \right) \left(\sin 2\beta + m_{\tilde{\chi}_1^0}/\mu \right)}{M_Z^3 c_w^2} \\ &\simeq \pm 0.01 \times e \tan \theta_w \frac{2\delta_1 m_{\tilde{\chi}_1^0}^3}{(1 + \delta_1) M_Z^3 c_w^2}, \end{aligned} \quad (\text{A.6})$$

$$\begin{aligned} C_{\tilde{\chi}_1^0\tilde{\chi}_1^0 Z} &\simeq 0.01 \times e \tan \theta_w \cos 2\beta \frac{\left(\mu^2 - m_{\tilde{\chi}_1^0}^2 \right)}{2M_Z^2 c_w^2} \\ &\simeq 0.01 \times e \tan \theta_w \cos 2\beta \frac{\delta_1 m_{\tilde{\chi}_1^0}^2}{M_Z^2 c_w^2}, \end{aligned} \quad (\text{A.7})$$

where μ is parameterized by $|\mu| = (1 + \delta_1)|m_{\tilde{\chi}_1^0}|$, with δ_1 denoting a small positive dimensionless number. These approximations indicate that the DM-nucleon scattering rates increase monotonously as the DM becomes heavier and/or $|\mu|$ departures from $|m_{\tilde{\chi}_1^0}|$. Specifically, for $m_{\tilde{\chi}_1^0} = 210$ GeV, which are the lower mass bound of the DM from the LHC search for Wino-dominated electroweakinos in the compressed mass spectrum case [90], we found that δ_1 must be less than about 0.26 to be consistent with the XENON-1T data on SI cross-section. For $m_{\tilde{\chi}_1^0} = 300$ GeV, it must be less than about 0.12. The Higgsinos in this narrow mass region contribute significantly to lepton signals at the LHC and the DM relic abundance. They also affect a_μ . Consequently, such a situation needs tuning to satisfy all experimental constraints.

- Case II: the DM co-annihilated with the Wino-dominated electroweakinos to obtain the measured abundance, and $|\mu|$ is much larger than $|m_{\tilde{\chi}_1^0}|$. This case predicts [112]:

$$C_1 \simeq \left(\mu^2 - m_{\tilde{\chi}_1^0}^2 \right)^2 \left(M_2 - m_{\tilde{\chi}_1^0} \right)^2, \quad (\text{A.8})$$

$$C_{\tilde{\chi}_1^0\tilde{\chi}_1^0 h} \simeq e \tan \theta_w \frac{M_Z \left(\sin 2\beta + m_{\tilde{\chi}_1^0}/\mu \right)}{\mu \left(1 - m_{\tilde{\chi}_1^0}^2/\mu^2 \right)}, \quad (\text{A.9})$$

$$C_{\tilde{\chi}_1^0\tilde{\chi}_1^0 Z} \simeq e \tan \theta_w \cos 2\beta \frac{M_Z^2}{2\mu^2 \left(1 - m_{\tilde{\chi}_1^0}^2/\mu^2 \right)}, \quad (\text{A.10})$$

and consequently the scattering rates decrease monotonously with the increase of $|\mu|$.

- Case III: the DM co-annihilated with the Higgsino-dominated electroweakinos to obtain the measured abundance, and $|M_2|$ is much larger than $|m_{\tilde{\chi}_1^0}|$. For this case:

$$\begin{aligned} C_1 &\simeq \left(\mu^2 - m_{\tilde{\chi}_1^0}^2\right)^2 \left(M_2 - m_{\tilde{\chi}_1^0}\right)^2 + \left(M_2 - m_{\tilde{\chi}_1^0}\right)^2 M_Z^2 s_w^2 \left(m_{\tilde{\chi}_1^0}^2 + \mu^2 + 2m_{\tilde{\chi}_1^0}\mu \sin 2\beta\right) \\ &\simeq \left(\mu^2 - m_{\tilde{\chi}_1^0}^2\right)^2 \left(M_2 - m_{\tilde{\chi}_1^0}\right)^2, \end{aligned} \quad (\text{A.11})$$

where the second approximation is obtained by assuming $|m_{\tilde{\chi}_1^0}| \gg m_Z$. Thus, $C_{\tilde{\chi}_1^0 \tilde{\chi}_1^0 h}$ and $C_{\tilde{\chi}_1^0 \tilde{\chi}_1^0 Z}$ have same approximations as those in Case-II. It should be noted that, because $m_{\tilde{\chi}_1^0}^2/\mu^2 \sim 1$, and consequently both $C_{\tilde{\chi}_1^0 \tilde{\chi}_1^0 h}$ and $C_{\tilde{\chi}_1^0 \tilde{\chi}_1^0 Z}$ are enhanced by the factor $1/(1 - m_{\tilde{\chi}_1^0}^2/\mu^2)$, the DM must be as massive as several TeV to be consistent with the XENON-1T results.

B Validation of CERN-EP-2021-059 (ATLAS_2106_01676)

Within the framework of CheckMATE-2.0.29, our codes were validated for all Signal Regions (SRs) in ATLAS_2106_01676 by considering $\tilde{\chi}_1^\pm \tilde{\chi}_2^0$ production at LHC. The masses of other charginos and neutralinos apart from the bino-like $\tilde{\chi}_1^0$ and wino-like $\tilde{\chi}_2^0$, $\tilde{\chi}_1^\pm$ were set to be 2.5 TeV, and $\tilde{\chi}_2^0$ and $\tilde{\chi}_1^\pm$ decay were set as follows: $\tilde{\chi}_2^0 \rightarrow \tilde{\chi}_1^0 Z/h$, $\tilde{\chi}_1^\pm \rightarrow \tilde{\chi}_1^0 W^\pm$. In the validation, 10^5 events were generated by the package MG5_aMC_v3_2_0 for the parameter point $(m_{\tilde{\chi}_1^\pm}/m_{\tilde{\chi}_2^0}, m_{\tilde{\chi}_1^0}) = (300\text{GeV}, 200\text{GeV})$.

In the proc_card.dat, the following setting was implemented:

```
import model MSSM_SLHA2 --modelname
generate p p > n2 x1+, n2 > z > l- l+ n1, x1+ > w+ > l+ vl n1
add process p p > n2 x1-, n2 > z > l- l+ n1, x1- > w- > l- vl~ n1
add process p p > n2 x1+ j j, n2 > z > l- l+ n1, x1+ > w+ > l+ vl n1
add process p p > n2 x1- j j, n2 > l- l+ n1, x1- > w- > l- vl~ n1
```

In the run_card.dat, the following setting was implemented and the others are kept default:

```
100000 = nevents ! Number of unweighted events requested.
0 = ickkw ! 0 no matching, 1 MLM
75.0 = ktdurham
```

In the param_card.dat, we set the following information and others are kept default:

```
Block mass
1000022 2.000000e+02 # Mneu1
```

```

1000023 3.000000e+02 # Mneu2
1000024 3.000000e+02 # Mch1
1000025 -2.50000e+03 # Mneu3
1000037 2.500000e+03 # Mch2
Block nmix # Neutralino Mixing Matrix ^M
1 1 9.86364430E-01 # N_11^M
1 2 -5.31103553E-02 # N_12^M
1 3 1.46433995E-01 # N_13^M
1 4 -5.31186117E-02 # N_14^M
2 1 9.93505358E-02 # N_21^M
2 2 9.44949299E-01 # N_22^M
2 3 -2.69846720E-01 # N_23^M
2 4 1.56150698E-01 # N_24^M
Block umix # Chargino Mixing Matrix U^M
1 1 9.16834859E-01 # U_11^M
1 2 -3.99266629E-01 # U_12^M
2 1 3.99266629E-01 # U_21^M
2 2 9.16834859E-01 # U_22^M
Block vmix # Chargino Mixing Matrix V^M
1 1 9.72557835E-01 # V_11^M
1 2 -2.32661249E-01 # V_12^M
2 1 2.32661249E-01 # V_21^M
2 2 9.72557835E-01 # V_22^M

```

In the pythia8_card.dat, we set:

```

Merging:Process = pp>{ch1-,1000015}{ch1+,-1000015}{n2, 1000023}
Merging:mayRemoveDecayProducts=on

```

Acknowledgement

This work is supported by the National Natural Science Foundation of China (NNSFC) under grant No. 12075076.

References

- [1] MUON G-2 collaboration, B. Abi et al., *Measurement of the Positive Muon Anomalous Magnetic Moment to 0.46 ppm*, *Phys. Rev. Lett.* **126** (2021) 141801 [[2104.03281](#)].
- [2] MUON G-2 collaboration, G. W. Bennett et al., *Final Report of the Muon E821 Anomalous Magnetic Moment Measurement at BNL*, *Phys. Rev. D* **73** (2006) 072003 [[hep-ex/0602035](#)].

- [3] T. Aoyama et al., *The anomalous magnetic moment of the muon in the Standard Model*, *Phys. Rept.* **887** (2020) 1 [[2006.04822](#)].
- [4] T. Aoyama, M. Hayakawa, T. Kinoshita and M. Nio, *Complete Tenth-Order QED Contribution to the Muon $g - 2$* , *Phys. Rev. Lett.* **109** (2012) 111808 [[1205.5370](#)].
- [5] T. Aoyama, T. Kinoshita and M. Nio, *Theory of the Anomalous Magnetic Moment of the Electron*, *Atoms* **7** (2019) 28.
- [6] A. Czarnecki, W. J. Marciano and A. Vainshtein, *Refinements in electroweak contributions to the muon anomalous magnetic moment*, *Phys. Rev.* **D67** (2003) 073006 [[hep-ph/0212229](#)].
- [7] C. Gnendiger, D. Stöckinger and H. Stöckinger-Kim, *The electroweak contributions to $(g - 2)_\mu$ after the Higgs boson mass measurement*, *Phys. Rev.* **D88** (2013) 053005 [[1306.5546](#)].
- [8] M. Davier, A. Hoecker, B. Malaescu and Z. Zhang, *Reevaluation of the hadronic vacuum polarisation contributions to the Standard Model predictions of the muon $g - 2$ and $\alpha(m_Z^2)$ using newest hadronic cross-section data*, *Eur. Phys. J.* **C77** (2017) 827 [[1706.09436](#)].
- [9] A. Keshavarzi, D. Nomura and T. Teubner, *Muon $g - 2$ and $\alpha(M_Z^2)$: a new data-based analysis*, *Phys. Rev.* **D97** (2018) 114025 [[1802.02995](#)].
- [10] G. Colangelo, M. Hoferichter and P. Stoffer, *Two-pion contribution to hadronic vacuum polarization*, *JHEP* **02** (2019) 006 [[1810.00007](#)].
- [11] M. Hoferichter, B.-L. Hoid and B. Kubis, *Three-pion contribution to hadronic vacuum polarization*, *JHEP* **08** (2019) 137 [[1907.01556](#)].
- [12] M. Davier, A. Hoecker, B. Malaescu and Z. Zhang, *A new evaluation of the hadronic vacuum polarisation contributions to the muon anomalous magnetic moment and to $\alpha(m_Z^2)$* , *Eur. Phys. J.* **C80** (2020) 241 [[1908.00921](#)].
- [13] A. Keshavarzi, D. Nomura and T. Teubner, *The $g - 2$ of charged leptons, $\alpha(M_Z^2)$ and the hyperfine splitting of muonium*, *Phys. Rev.* **D101** (2020) 014029 [[1911.00367](#)].
- [14] A. Kurz, T. Liu, P. Marquard and M. Steinhauser, *Hadronic contribution to the muon anomalous magnetic moment to next-to-next-to-leading order*, *Phys. Lett.* **B734** (2014) 144 [[1403.6400](#)].
- [15] K. Melnikov and A. Vainshtein, *Hadronic light-by-light scattering contribution to the muon anomalous magnetic moment revisited*, *Phys. Rev.* **D70** (2004) 113006 [[hep-ph/0312226](#)].
- [16] P. Masjuan and P. Sánchez-Puertas, *Pseudoscalar-pole contribution to the $(g_\mu - 2)$: a rational approach*, *Phys. Rev.* **D95** (2017) 054026 [[1701.05829](#)].
- [17] G. Colangelo, M. Hoferichter, M. Procura and P. Stoffer, *Dispersion relation for hadronic light-by-light scattering: two-pion contributions*, *JHEP* **04** (2017) 161 [[1702.07347](#)].

- [18] M. Hoferichter, B.-L. Hoid, B. Kubis, S. Leupold and S. P. Schneider, *Dispersion relation for hadronic light-by-light scattering: pion pole*, *JHEP* **10** (2018) 141 [[1808.04823](#)].
- [19] A. Gérardin, H. B. Meyer and A. Nyffeler, *Lattice calculation of the pion transition form factor with $N_f = 2 + 1$ Wilson quarks*, *Phys. Rev. D* **100** (2019) 034520 [[1903.09471](#)].
- [20] J. Bijnens, N. Hermansson-Truedsson and A. Rodríguez-Sánchez, *Short-distance constraints for the $HLbL$ contribution to the muon anomalous magnetic moment*, *Phys. Lett. B* **798** (2019) 134994 [[1908.03331](#)].
- [21] G. Colangelo, F. Hagelstein, M. Hoferichter, L. Laub and P. Stoffer, *Longitudinal short-distance constraints for the hadronic light-by-light contribution to $(g - 2)_\mu$ with large- N_c Regge models*, *JHEP* **03** (2020) 101 [[1910.13432](#)].
- [22] T. Blum, N. Christ, M. Hayakawa, T. Izubuchi, L. Jin, C. Jung et al., *The hadronic light-by-light scattering contribution to the muon anomalous magnetic moment from lattice QCD*, *Phys. Rev. Lett.* **124** (2020) 132002 [[1911.08123](#)].
- [23] G. Colangelo, M. Hoferichter, A. Nyffeler, M. Passera and P. Stoffer, *Remarks on higher-order hadronic corrections to the muon $g - 2$* , *Phys. Lett. B* **735** (2014) 90 [[1403.7512](#)].
- [24] P. Athron, C. Balázs, D. H. Jacob, W. Kotlarski, D. Stöckinger and H. Stöckinger-Kim, *New physics explanations of a_μ in light of the FNAL muon $g - 2$ measurement*, [2104.03691](#).
- [25] P. Fayet and S. Ferrara, *Supersymmetry*, *Phys. Rept.* **32** (1977) 249.
- [26] H. E. Haber and G. L. Kane, *The Search for Supersymmetry: Probing Physics Beyond the Standard Model*, *Phys. Rept.* **117** (1985) 75.
- [27] S. P. Martin, *A Supersymmetry primer*, [hep-ph/9709356](#).
- [28] G. Jungman, M. Kamionkowski and K. Griest, *Supersymmetric dark matter*, *Phys. Rept.* **267** (1996) 195 [[hep-ph/9506380](#)].
- [29] S. P. Martin and J. D. Wells, *Muon Anomalous Magnetic Dipole Moment in Supersymmetric Theories*, *Phys. Rev. D* **64** (2001) 035003 [[hep-ph/0103067](#)].
- [30] F. Domingo and U. Ellwanger, *Constraints from the Muon $g-2$ on the Parameter Space of the NMSSM*, *JHEP* **07** (2008) 079 [[0806.0733](#)].
- [31] T. Moroi, *The Muon anomalous magnetic dipole moment in the minimal supersymmetric standard model*, *Phys. Rev. D* **53** (1996) 6565 [[hep-ph/9512396](#)].
- [32] W. Hollik, J. I. Illana, S. Rigolin and D. Stockinger, *One loop MSSM contribution to the weak magnetic dipole moments of heavy fermions*, *Phys. Lett. B* **416** (1998) 345 [[hep-ph/9707437](#)].
- [33] P. Athron, M. Bach, H. G. Fargnoli, C. Gnendiger, R. Greifenhagen, J.-h. Park

- et al., *GM2Calc: Precise MSSM prediction for $(g - 2)$ of the muon*, *Eur. Phys. J. C* **76** (2016) 62 [[1510.08071](#)].
- [34] M. Endo, K. Hamaguchi, S. Iwamoto and T. Kitahara, *Supersymmetric interpretation of the muon $g - 2$ anomaly*, *JHEP* **07** (2021) 075 [[2104.03217](#)].
- [35] D. Stockinger, *The Muon Magnetic Moment and Supersymmetry*, *J. Phys. G* **34** (2007) R45 [[hep-ph/0609168](#)].
- [36] A. Czarnecki and W. J. Marciano, *The Muon anomalous magnetic moment: A Harbinger for 'new physics'*, *Phys. Rev. D* **64** (2001) 013014 [[hep-ph/0102122](#)].
- [37] J. Cao, Z. Heng, D. Li and J. M. Yang, *Current experimental constraints on the lightest Higgs boson mass in the constrained MSSM*, *Phys. Lett. B* **710** (2012) 665 [[1112.4391](#)].
- [38] Z. Kang, *$H_{u,d}$ -messenger Couplings Address the $\mu/B_\mu \setminus \mathcal{E} A_t/m_{H_u}^2$ Problem and $(g - 2)_\mu$ Puzzle*, [1610.06024](#).
- [39] B. Zhu, R. Ding and T. Li, *Higgs mass and muon anomalous magnetic moment in the MSSM with gauge-gravity hybrid mediation*, *Phys. Rev. D* **96** (2017) 035029 [[1610.09840](#)].
- [40] T. T. Yanagida and N. Yokozaki, *Muon $g - 2$ in MSSM gauge mediation revisited*, *Phys. Lett. B* **772** (2017) 409 [[1704.00711](#)].
- [41] K. Hagiwara, K. Ma and S. Mukhopadhyay, *Closing in on the chargino contribution to the muon $g-2$ in the MSSM: current LHC constraints*, *Phys. Rev. D* **97** (2018) 055035 [[1706.09313](#)].
- [42] P. Cox, C. Han and T. T. Yanagida, *Muon $g - 2$ and dark matter in the minimal supersymmetric standard model*, *Phys. Rev. D* **98** (2018) 055015 [[1805.02802](#)].
- [43] H. M. Tran and H. T. Nguyen, *GUT-inspired MSSM in light of muon $g - 2$ and LHC results at $\sqrt{s} = 13$ TeV*, *Phys. Rev. D* **99** (2019) 035040 [[1812.11757](#)].
- [44] B. P. Padley, K. Sinha and K. Wang, *Natural Supersymmetry, Muon $g - 2$, and the Last Crevices for the Top Squark*, *Phys. Rev. D* **92** (2015) 055025 [[1505.05877](#)].
- [45] A. Choudhury, L. Darmé, L. Roszkowski, E. M. Sessolo and S. Trojanowski, *Muon $g - 2$ and related phenomenology in constrained vector-like extensions of the MSSM*, *JHEP* **05** (2017) 072 [[1701.08778](#)].
- [46] N. Okada and H. M. Tran, *125 GeV Higgs boson mass and muon $g - 2$ in 5D MSSM*, *Phys. Rev. D* **94** (2016) 075016 [[1606.05329](#)].
- [47] X. Du and F. Wang, *NMSSM From Alternative Deflection in Generalized Deflected Anomaly Mediated SUSY Breaking*, *Eur. Phys. J. C* **78** (2018) 431 [[1710.06105](#)].
- [48] X. Ning and F. Wang, *Solving the muon $g-2$ anomaly within the NMSSM from generalized deflected AMSB*, *JHEP* **08** (2017) 089 [[1704.05079](#)].
- [49] K. Wang, F. Wang, J. Zhu and Q. Jie, *The semi-constrained NMSSM in light of*

- muon $g-2$, LHC, and dark matter constraints*, *Chin. Phys. C* **42** (2018) 103109 [[1811.04435](#)].
- [50] J.-L. Yang, T.-F. Feng, Y.-L. Yan, W. Li, S.-M. Zhao and H.-B. Zhang, *Lepton-flavor violation and two loop electroweak corrections to $(g-2)_\mu$ in the B - L symmetric SSM*, *Phys. Rev. D* **99** (2019) 015002 [[1812.03860](#)].
 - [51] C.-X. Liu, H.-B. Zhang, J.-L. Yang, S.-M. Zhao, Y.-B. Liu and T.-F. Feng, *Higgs boson decay $h \rightarrow Z\gamma$ and muon magnetic dipole moment in the $\mu\nu$ SSM*, *JHEP* **04** (2020) 002 [[2002.04370](#)].
 - [52] J. Cao, J. Lian, L. Meng, Y. Yue and P. Zhu, *Anomalous muon magnetic moment in the inverse seesaw extended next-to-minimal supersymmetric standard model*, *Phys. Rev. D* **101** (2020) 095009 [[1912.10225](#)].
 - [53] J. Cao, Y. He, J. Lian, D. Zhang and P. Zhu, *Electron and muon anomalous magnetic moments in the inverse seesaw extended NMSSM*, *Phys. Rev. D* **104** (2021) 055009 [[2102.11355](#)].
 - [54] W. Ke and P. Slavich, *Higgs-mass constraints on a supersymmetric solution of the muon $g-2$ anomaly*, [2109.15277](#).
 - [55] J. L. Lamborn, T. Li, J. A. Maxin and D. V. Nanopoulos, *Resolving the $(g-2)_\mu$ Discrepancy with \mathcal{F} - $SU(5)$ Intersecting D -branes*, [2108.08084](#).
 - [56] S. Li, Y. Xiao and J. M. Yang, *Constraining CP -phases in SUSY: an interplay of muon/electron $g-2$ and electron EDM*, [2108.00359](#).
 - [57] Y. Nakai, M. Reece and M. Suzuki, *Supersymmetric alignment models for $(g-2)_\mu$* , *JHEP* **10** (2021) 068 [[2107.10268](#)].
 - [58] S. Li, Y. Xiao and J. M. Yang, *Can electron and muon $g-2$ anomalies be jointly explained in SUSY?*, [2107.04962](#).
 - [59] J. S. Kim, D. E. Lopez-Fogliani, A. D. Perez and R. R. de Austri, *The new $(g-2)_\mu$ and Right-Handed Sneutrino Dark Matter*, [2107.02285](#).
 - [60] Z. Li, G.-L. Liu, F. Wang, J. M. Yang and Y. Zhang, *Gluino-SUGRA scenarios in light of FNAL muon $g-2$ anomaly*, [2106.04466](#).
 - [61] W. Altmannshofer, S. A. Gadam, S. Gori and N. Hamer, *Explaining $(g-2)_\mu$ with Multi-TeV Sleptons*, [2104.08293](#).
 - [62] H. Baer, V. Barger and H. Serce, *Anomalous muon magnetic moment, supersymmetry, naturalness, LHC search limits and the landscape*, *Phys. Lett. B* **820** (2021) 136480 [[2104.07597](#)].
 - [63] M. Chakraborti, L. Roszkowski and S. Trojanowski, *GUT-constrained supersymmetry and dark matter in light of the new $(g-2)_\mu$ determination*, *JHEP* **05** (2021) 252 [[2104.04458](#)].
 - [64] A. Aboubrahim, M. Klasen and P. Nath, *What the Fermilab muon $g-2$ experiment*

tells us about discovering supersymmetry at high luminosity and high energy upgrades to the LHC, *Phys. Rev. D* **104** (2021) 035039 [[2104.03839](#)].

- [65] S. Iwamoto, T. T. Yanagida and N. Yokozaki, *Wino-Higgsino dark matter in MSSM from the $g-2$ anomaly*, *Phys. Lett. B* **823** (2021) 136768 [[2104.03223](#)].
- [66] M. Chakraborti, S. Heinemeyer and I. Saha, *The new "MUON $G-2$ " Result and Supersymmetry*, [2104.03287](#).
- [67] J. Cao, J. Lian, Y. Pan, D. Zhang and P. Zhu, *Improved $(g-2)_\mu$ measurement and singlino dark matter in μ -term extended \mathbb{Z}_3 -NMSSM*, *JHEP* **09** (2021) 175 [[2104.03284](#)].
- [68] W. Yin, *Muon $g-2$ anomaly in anomaly mediation*, *JHEP* **06** (2021) 029 [[2104.03259](#)].
- [69] H.-B. Zhang, C.-X. Liu, J.-L. Yang and T.-F. Feng, *Muon anomalous magnetic dipole moment in the $\mu\nu$ SSM*, [2104.03489](#).
- [70] M. Ibe, S. Kobayashi, Y. Nakayama and S. Shirai, *Muon $g-2$ in Gauge Mediation without SUSY CP Problem*, [2104.03289](#).
- [71] C. Han, *Muon $g-2$ and CP violation in MSSM*, [2104.03292](#).
- [72] F. Wang, L. Wu, Y. Xiao, J. M. Yang and Y. Zhang, *GUT-scale constrained SUSY in light of new muon $g-2$ measurement*, *Nucl. Phys. B* **970** (2021) 115486 [[2104.03262](#)].
- [73] M.-D. Zheng and H.-H. Zhang, *Studying the $b \rightarrow s\ell + \ell^-$ anomalies and $(g-2)_\mu$ in R -parity violating MSSM framework with the inverse seesaw mechanism*, *Phys. Rev. D* **104** (2021) 115023.
- [74] M. Chakraborti, S. Heinemeyer, I. Saha and C. Schappacher, *$(g-2)_\mu$ and SUSY Dark Matter: Direct Detection and Collider Search Complementarity*, [2112.01389](#).
- [75] A. Aboubrahim, M. Klasen, P. Nath and R. M. Syed, *Tests of gluino-driven radiative breaking of the electroweak symmetry at the LHC*, in *10th International Conference on New Frontiers in Physics*, 12, 2021, [2112.04986](#).
- [76] M. I. Ali, M. Chakraborti, U. Chattopadhyay and S. Mukherjee, *Muon and Electron $(g-2)$ Anomalies with Non-Holomorphic Interactions in MSSM*, [2112.09867](#).
- [77] K. Wang and J. Zhu, *A smuon in the NMSSM confronted with the muon $g-2$ and SUSY searches*, [2112.14576](#).
- [78] M. Chakraborti, S. Heinemeyer and I. Saha, *Improved $(g-2)_\mu$ Measurements and Supersymmetry*, *Eur. Phys. J. C* **80** (2020) 984 [[2006.15157](#)].
- [79] S. Baum, M. Carena, N. R. Shah and C. E. M. Wagner, *The tiny $(g-2)$ muon wobble from small- μ supersymmetry*, *JHEP* **01** (2022) 025 [[2104.03302](#)].
- [80] XENON collaboration, E. Aprile et al., *Dark Matter Search Results from a One Ton-Year Exposure of XENON1T*, *Phys. Rev. Lett.* **121** (2018) 111302 [[1805.12562](#)].

- [81] XENON collaboration, E. Aprile et al., *Constraining the spin-dependent WIMP-nucleon cross sections with XENON1T*, *Phys. Rev. Lett.* **122** (2019) 141301 [[1902.03234](#)].
- [82] PANDAX-II collaboration, C. Cheng et al., *Search for Light Dark Matter-Electron Scatterings in the PandaX-II Experiment*, *Phys. Rev. Lett.* **126** (2021) 211803 [[2101.07479](#)].
- [83] PANDAX-4T collaboration, Y. Meng et al., *Dark Matter Search Results from the PandaX-4T Commissioning Run*, [2107.13438](#).
- [84] ATLAS collaboration, G. Aad et al., *Search for chargino-neutralino production with mass splittings near the electroweak scale in three-lepton final states in $\sqrt{s}=13$ TeV pp collisions with the ATLAS detector*, *Phys. Rev. D* **101** (2020) 072001 [[1912.08479](#)].
- [85] ATLAS collaboration, G. Aad et al., *Search for electroweak production of charginos and sleptons decaying into final states with two leptons and missing transverse momentum in $\sqrt{s} = 13$ TeV pp collisions using the ATLAS detector*, *Eur. Phys. J. C* **80** (2020) 123 [[1908.08215](#)].
- [86] ATLAS collaboration, G. Aad et al., *Search for direct production of electroweakinos in final states with one lepton, missing transverse momentum and a Higgs boson decaying into two b-jets in pp collisions at $\sqrt{s} = 13$ TeV with the ATLAS detector*, *Eur. Phys. J. C* **80** (2020) 691 [[1909.09226](#)].
- [87] CMS collaboration, A. M. Sirunyan et al., *Search for supersymmetric partners of electrons and muons in proton-proton collisions at $\sqrt{s} = 13$ TeV*, *Phys. Lett. B* **790** (2019) 140 [[1806.05264](#)].
- [88] CMS collaboration, A. M. Sirunyan et al., *Combined search for electroweak production of charginos and neutralinos in proton-proton collisions at $\sqrt{s} = 13$ TeV*, *JHEP* **03** (2018) 160 [[1801.03957](#)].
- [89] ATLAS collaboration, G. Aad et al., *Searches for electroweak production of supersymmetric particles with compressed mass spectra in $\sqrt{s} = 13$ TeV pp collisions with the ATLAS detector*, *Phys. Rev. D* **101** (2020) 052005 [[1911.12606](#)].
- [90] ATLAS collaboration, G. Aad et al., *Search for chargino-neutralino pair production in final states with three leptons and missing transverse momentum in $\sqrt{s} = 13$ TeV pp collisions with the ATLAS detector*, [2106.01676](#).
- [91] CMS collaboration, A. M. Sirunyan et al., *Search for supersymmetry in final states with two oppositely charged same-flavor leptons and missing transverse momentum in proton-proton collisions at $\sqrt{s} = 13$ TeV*, *JHEP* **04** (2021) 123 [[2012.08600](#)].
- [92] G. R. Farrar and P. Fayet, *Phenomenology of the Production, Decay, and Detection of New Hadronic States Associated with Supersymmetry*, *Phys. Lett. B* **76** (1978) 575.

- [93] J. F. Gunion and H. E. Haber, *Higgs Bosons in Supersymmetric Models. 1.*, *Nucl. Phys. B* **272** (1986) 1.
- [94] A. Djouadi, *The Anatomy of electro-weak symmetry breaking. II. The Higgs bosons in the minimal supersymmetric model*, *Phys. Rept.* **459** (2008) 1 [[hep-ph/0503173](#)].
- [95] PLANCK collaboration, N. Aghanim et al., *Planck 2018 results. VI. Cosmological parameters*, *Astron. Astrophys.* **641** (2020) A6 [[1807.06209](#)].
- [96] E. Bagnaschi et al., *Likelihood Analysis of the pMSSM11 in Light of LHC 13-TeV Data*, *Eur. Phys. J. C* **78** (2018) 256 [[1710.11091](#)].
- [97] H. Baer, V. Barger, P. Huang and X. Tata, *Natural Supersymmetry: LHC, dark matter and ILC searches*, *JHEP* **05** (2012) 109 [[1203.5539](#)].
- [98] CMS collaboration, A. M. Sirunyan et al., *Searches for physics beyond the standard model with the M_{T2} variable in hadronic final states with and without disappearing tracks in proton-proton collisions at $\sqrt{s} = 13$ TeV*, *Eur. Phys. J. C* **80** (2020) 3 [[1909.03460](#)].
- [99] J. Cao, Y. He, L. Shang, Y. Zhang and P. Zhu, *Current status of a natural NMSSM in light of LHC 13 TeV data and XENON-1T results*, *Phys. Rev.* **D99** (2019) 075020 [[1810.09143](#)].
- [100] ATLAS collaboration, G. Aad et al., *Search for charged Higgs bosons decaying into a top quark and a bottom quark at $\sqrt{s} = 13$ TeV with the ATLAS detector*, *JHEP* **06** (2021) 145 [[2102.10076](#)].
- [101] U. Ellwanger, C. Hugonie and A. M. Teixeira, *The Next-to-Minimal Supersymmetric Standard Model*, *Phys. Rept.* **496** (2010) 1 [[0910.1785](#)].
- [102] M. Maniatis, *The Next-to-Minimal Supersymmetric extension of the Standard Model reviewed*, *Int. J. Mod. Phys. A* **25** (2010) 3505 [[0906.0777](#)].
- [103] J. Cao, Y. He, L. Shang, W. Su and Y. Zhang, *Natural NMSSM after LHC Run I and the Higgsino dominated dark matter scenario*, *JHEP* **08** (2016) 037 [[1606.04416](#)].
- [104] U. Ellwanger, *Present Status and Future Tests of the Higgsino-Singlino Sector in the NMSSM*, *JHEP* **02** (2017) 051 [[1612.06574](#)].
- [105] Q.-F. Xiang, X.-J. Bi, P.-F. Yin and Z.-H. Yu, *Searching for Singlino-Higgsino Dark Matter in the NMSSM*, *Phys. Rev. D* **94** (2016) 055031 [[1606.02149](#)].
- [106] S. Baum, M. Carena, N. R. Shah and C. E. Wagner, *Higgs portals for thermal Dark Matter. EFT perspectives and the NMSSM*, *JHEP* **04** (2018) 069 [[1712.09873](#)].
- [107] U. Ellwanger and C. Hugonie, *The higgsino–singlino sector of the NMSSM: combined constraints from dark matter and the LHC*, *Eur. Phys. J. C* **78** (2018) 735 [[1806.09478](#)].
- [108] F. Domingo, J. S. Kim, V. M. Lozano, P. Martin-Ramiro and R. Ruiz de Austri,

Confronting the neutralino and chargino sector of the NMSSM with the multilepton searches at the LHC, *Phys. Rev. D* **101** (2020) 075010 [[1812.05186](#)].

- [109] S. Baum, N. R. Shah and K. Freese, *The NMSSM is within Reach of the LHC: Mass Correlations & Decay Signatures*, *JHEP* **04** (2019) 011 [[1901.02332](#)].
- [110] M. van Beekveld, S. Caron and R. Ruiz de Austri, *The current status of fine-tuning in supersymmetry*, *JHEP* **01** (2020) 147 [[1906.10706](#)].
- [111] W. Abdallah, A. Chatterjee and A. Datta, *Revisiting singlino dark matter of the natural Z_3 -symmetric NMSSM in the light of LHC*, *JHEP* **09** (2019) 095 [[1907.06270](#)].
- [112] J. Cao, L. Meng, Y. Yue, H. Zhou and P. Zhu, *Suppressing the scattering of wimp dark matter and nucleons in supersymmetric theories*, *Phys. Rev. D* **101** (2020) 075003.
- [113] M. Guchait and A. Roy, *Light Singlino Dark Matter at the LHC*, *Phys. Rev. D* **102** (2020) 075023 [[2005.05190](#)].
- [114] W. Abdallah, A. Datta and S. Roy, *A relatively light, highly bino-like dark matter in the Z_3 -symmetric NMSSM and recent LHC searches*, *JHEP* **04** (2021) 122 [[2012.04026](#)].
- [115] H. Zhou, J. Cao, J. Lian and D. Zhang, *Singlino-dominated dark matter in Z_3 -symmetric NMSSM*, *Phys. Rev. D* **104** (2021) 015017 [[2102.05309](#)].
- [116] J. Cao, D. Li, J. Lian, Y. Yue and H. Zhou, *Singlino-dominated dark matter in general NMSSM*, *JHEP* **06** (2021) 176 [[2102.05317](#)].
- [117] U. Ellwanger, *Nonrenormalizable interactions from supergravity, quantum corrections and effective low-energy theories*, *Phys. Lett. B* **133** (1983) 187.
- [118] S. A. Abel, *Destabilizing divergences in the NMSSM*, *Nucl. Phys. B* **480** (1996) 55 [[hep-ph/9609323](#)].
- [119] C. F. Kolda, S. Pokorski and N. Polonsky, *Stabilized singlets in supergravity as a source of the μ - parameter*, *Phys. Rev. Lett.* **80** (1998) 5263 [[hep-ph/9803310](#)].
- [120] C. Panagiotakopoulos and K. Tamvakis, *Stabilized NMSSM without domain walls*, *Phys. Lett. B* **446** (1999) 224 [[hep-ph/9809475](#)].
- [121] G. G. Ross and K. Schmidt-Hoberg, *The Fine-Tuning of the Generalised NMSSM*, *Nucl. Phys. B* **862** (2012) 710 [[1108.1284](#)].
- [122] H. M. Lee, S. Raby, M. Ratz, G. G. Ross, R. Schieren, K. Schmidt-Hoberg et al., *A unique \mathbb{Z}_4^R symmetry for the MSSM*, *Phys. Lett. B* **694** (2011) 491 [[1009.0905](#)].
- [123] H. M. Lee, S. Raby, M. Ratz, G. G. Ross, R. Schieren, K. Schmidt-Hoberg et al., *Discrete R symmetries for the MSSM and its singlet extensions*, *Nucl. Phys. B* **850** (2011) 1 [[1102.3595](#)].
- [124] G. G. Ross, K. Schmidt-Hoberg and F. Staub, *The Generalised NMSSM at One Loop: Fine Tuning and Phenomenology*, *JHEP* **08** (2012) 074 [[1205.1509](#)].

- [125] J.-J. Cao, Z.-X. Heng, J. M. Yang, Y.-M. Zhang and J.-Y. Zhu, *A SM-like Higgs near 125 GeV in low energy SUSY: a comparative study for MSSM and NMSSM*, *JHEP* **03** (2012) 086 [[1202.5821](#)].
- [126] S. Ferrara, R. Kallosh, A. Linde, A. Marrani and A. Van Proeyen, *Jordan Frame Supergravity and Inflation in NMSSM*, *Phys. Rev. D* **82** (2010) 045003 [[1004.0712](#)].
- [127] S. Ferrara, R. Kallosh, A. Linde, A. Marrani and A. Van Proeyen, *Superconformal Symmetry, NMSSM, and Inflation*, *Phys. Rev. D* **83** (2011) 025008 [[1008.2942](#)].
- [128] M. B. Einhorn and D. R. T. Jones, *Inflation with Non-minimal Gravitational Couplings in Supergravity*, *JHEP* **03** (2010) 026 [[0912.2718](#)].
- [129] W. G. Hollik, S. Liebler, G. Moortgat-Pick, S. Paßehr and G. Weiglein, *Phenomenology of the inflation-inspired NMSSM at the electroweak scale*, *Eur. Phys. J. C* **79** (2019) 75 [[1809.07371](#)].
- [130] W. G. Hollik, C. Li, G. Moortgat-Pick and S. Paasch, *Phenomenology of a Supersymmetric Model Inspired by Inflation*, *Eur. Phys. J. C* **81** (2021) 141 [[2004.14852](#)].
- [131] C. Cheung, M. Papucci, D. Sanford, N. R. Shah and K. M. Zurek, *NMSSM Interpretation of the Galactic Center Excess*, *Phys. Rev. D* **90** (2014) 075011 [[1406.6372](#)].
- [132] M. Badziak, M. Olechowski and P. Szczerbiak, *Blind spots for neutralino dark matter in the NMSSM*, *JHEP* **03** (2016) 179 [[1512.02472](#)].
- [133] M. Badziak, M. Olechowski and P. Szczerbiak, *Spin-dependent constraints on blind spots for thermal singlino-higgsino dark matter with(out) light singlets*, *Journal of High Energy Physics* **2017** (2017) .
- [134] M. Pospelov, A. Ritz and M. B. Voloshin, *Secluded WIMP Dark Matter*, *Phys. Lett. B* **662** (2008) 53 [[0711.4866](#)].
- [135] F. Feroz, M. P. Hobson and M. Bridges, *MultiNest: an efficient and robust Bayesian inference tool for cosmology and particle physics*, *Mon. Not. Roy. Astron. Soc.* **398** (2009) 1601 [[0809.3437](#)].
- [136] F. Staub, *SARAH*, [0806.0538](#).
- [137] F. Staub, *SARAH 3.2: Dirac Gauginos, UFO output, and more*, *Comput. Phys. Commun.* **184** (2013) 1792 [[1207.0906](#)].
- [138] F. Staub, *SARAH 4 : A tool for (not only SUSY) model builders*, *Comput. Phys. Commun.* **185** (2014) 1773 [[1309.7223](#)].
- [139] F. Staub, *Exploring new models in all detail with SARAH*, *Adv. High Energy Phys.* **2015** (2015) 840780 [[1503.04200](#)].
- [140] W. Porod, *SPheno, a program for calculating supersymmetric spectra, SUSY particle decays and SUSY particle production at e+ e- colliders*, *Comput. Phys. Commun.* **153** (2003) 275 [[hep-ph/0301101](#)].

- [141] W. Porod and F. Staub, *SPheno 3.1: Extensions including flavour, CP-phases and models beyond the MSSM*, *Comput. Phys. Commun.* **183** (2012) 2458 [[1104.1573](#)].
- [142] W. Porod, F. Staub and A. Vicente, *A Flavor Kit for BSM models*, *Eur. Phys. J. C* **74** (2014) 2992 [[1405.1434](#)].
- [143] G. Belanger, F. Boudjema, A. Pukhov and A. Semenov, *MicrOMEGAs: A Program for calculating the relic density in the MSSM*, *Comput. Phys. Commun.* **149** (2002) 103 [[hep-ph/0112278](#)].
- [144] G. Belanger, F. Boudjema, C. Hugonie, A. Pukhov and A. Semenov, *Relic density of dark matter in the NMSSM*, *JCAP* **09** (2005) 001 [[hep-ph/0505142](#)].
- [145] G. Belanger, F. Boudjema, A. Pukhov and A. Semenov, *MicrOMEGAs 2.0: A Program to calculate the relic density of dark matter in a generic model*, *Comput. Phys. Commun.* **176** (2007) 367 [[hep-ph/0607059](#)].
- [146] G. Belanger, F. Boudjema, A. Pukhov and A. Semenov, *micrOMEGAs: A Tool for dark matter studies*, *Nuovo Cim. C* **033N2** (2010) 111 [[1005.4133](#)].
- [147] G. Belanger, F. Boudjema, A. Pukhov and A. Semenov, *micrOMEGAs_3: A program for calculating dark matter observables*, *Comput. Phys. Commun.* **185** (2014) 960 [[1305.0237](#)].
- [148] D. Barducci, G. Belanger, J. Bernon, F. Boudjema, J. Da Silva, S. Kraml et al., *Collider limits on new physics within micrOMEGAs_4.3*, *Comput. Phys. Commun.* **222** (2018) 327 [[1606.03834](#)].
- [149] PLANCK collaboration, N. Aghanim et al., *Planck 2018 results. VI. Cosmological parameters*, *Astron. Astrophys.* **641** (2020) A6 [[1807.06209](#)].
- [150] XENON collaboration, E. Aprile et al., *Dark Matter Search Results from a One Ton-Year Exposure of XENON1T*, *Phys. Rev. Lett.* **121** (2018) 111302 [[1805.12562](#)].
- [151] XENON collaboration, E. Aprile et al., *Constraining the spin-dependent WIMP-nucleon cross sections with XENON1T*, *Phys. Rev. Lett.* **122** (2019) 141301 [[1902.03234](#)].
- [152] FERMI-LAT collaboration, M. Ackermann et al., *Searching for Dark Matter Annihilation from Milky Way Dwarf Spheroidal Galaxies with Six Years of Fermi Large Area Telescope Data*, *Phys. Rev. Lett.* **115** (2015) 231301 [[1503.02641](#)].
- [153] L. M. Carpenter, R. Colburn, J. Goodman and T. Linden, *Indirect Detection Constraints on s and t Channel Simplified Models of Dark Matter*, *Phys. Rev. D* **94** (2016) 055027 [[1606.04138](#)].
- [154] P. Bechtle, S. Heinemeyer, O. Stål, T. Stefaniak and G. Weiglein, *Probing the Standard Model with Higgs signal rates from the Tevatron, the LHC and a future ILC*, *JHEP* **11** (2014) 039 [[1403.1582](#)].
- [155] P. Bechtle, S. Heinemeyer, O. Stal, T. Stefaniak and G. Weiglein, *Applying*

- Exclusion Likelihoods from LHC Searches to Extended Higgs Sectors*, *Eur. Phys. J. C* **75** (2015) 421 [[1507.06706](#)].
- [156] PARTICLE DATA GROUP collaboration, M. Tanabashi, K. Hagiwara, Hikasa et al., *Review of particle physics*, *Phys. Rev. D* **98** (2018) 030001.
- [157] C. K. Khosa, S. Kraml, A. Lessa, P. Neuhuber and W. Waltenberger, *SModelS database update v1.2.3*, [2005.00555](#).
- [158] M. Drees, H. Dreiner, D. Schmeier, J. Tattersall and J. S. Kim, *CheckMATE: Confronting your Favourite New Physics Model with LHC Data*, *Comput. Phys. Commun.* **187** (2015) 227 [[1312.2591](#)].
- [159] D. Dercks, N. Desai, J. S. Kim, K. Rolbiecki, J. Tattersall and T. Weber, *CheckMATE 2: From the model to the limit*, *Comput. Phys. Commun.* **221** (2017) 383 [[1611.09856](#)].
- [160] J. S. Kim, D. Schmeier, J. Tattersall and K. Rolbiecki, *A framework to create customised LHC analyses within CheckMATE*, *Comput. Phys. Commun.* **196** (2015) 535 [[1503.01123](#)].
- [161] J. E. Camargo-Molina, B. O’Leary, W. Porod and F. Staub, *Vevacious: A Tool For Finding The Global Minima Of One-Loop Effective Potentials With Many Scalars*, *Eur. Phys. J. C* **73** (2013) 2588 [[1307.1477](#)].
- [162] J. E. Camargo-Molina, B. Garbrecht, B. O’Leary, W. Porod and F. Staub, *Constraining the Natural MSSM through tunneling to color-breaking vacua at zero and non-zero temperature*, *Phys. Lett. B* **737** (2014) 156 [[1405.7376](#)].
- [163] A. Fowlie and M. H. Bardsley, *Superplot: a graphical interface for plotting and analysing MultiNest output*, *Eur. Phys. J. Plus* **131** (2016) 391 [[1603.00555](#)].
- [164] J. Cao, J. Li, Y. Pan, L. Shang, Y. Yue and D. Zhang, *Bayesian analysis of sneutrino dark matter in the NMSSM with a type-I seesaw mechanism*, *Phys. Rev. D* **99** (2019) 115033 [[1807.03762](#)].
- [165] J. L. Hintze and R. D. Nelson, *Violin plots: a box plot-density trace synergism*, *The American Statistician* **52** (1998) 181.
- [166] W. Beenakker, R. Hopker and M. Spira, *PROSPINO: A Program for the production of supersymmetric particles in next-to-leading order QCD*, [hep-ph/9611232](#).
- [167] J. Alwall, M. Herquet, F. Maltoni, O. Mattelaer and T. Stelzer, *MadGraph 5 : Going Beyond*, *JHEP* **06** (2011) 128 [[1106.0522](#)].
- [168] E. Conte, B. Fuks and G. Serret, *MadAnalysis 5, A User-Friendly Framework for Collider Phenomenology*, *Comput. Phys. Commun.* **184** (2013) 222 [[1206.1599](#)].
- [169] T. Sjöstrand, S. Ask, J. R. Christiansen, R. Corke, N. Desai, P. Ilten et al., *An introduction to PYTHIA 8.2*, *Comput. Phys. Commun.* **191** (2015) 159 [[1410.3012](#)].
- [170] DELPHES 3 collaboration, J. de Favereau, C. Delaere, P. Demin, A. Giammanco,

- V. Lemaître, A. Mertens et al., *DELPHES 3, A modular framework for fast simulation of a generic collider experiment*, *JHEP* **02** (2014) 057 [[1307.6346](#)].
- [171] ATLAS collaboration, M. Aaboud et al., *Search for electroweak production of supersymmetric particles in final states with two or three leptons at $\sqrt{s} = 13$ TeV with the ATLAS detector*, *Eur. Phys. J. C* **78** (2018) 995 [[1803.02762](#)].
- [172] ATLAS collaboration, M. Aaboud et al., *Search for photonic signatures of gauge-mediated supersymmetry in 13 TeV pp collisions with the ATLAS detector*, *Phys. Rev. D* **97** (2018) 092006 [[1802.03158](#)].
- [173] ATLAS collaboration, M. Aaboud et al., *Search for electroweak production of supersymmetric states in scenarios with compressed mass spectra at $\sqrt{s} = 13$ TeV with the ATLAS detector*, *Phys. Rev. D* **97** (2018) 052010 [[1712.08119](#)].
- [174] CMS collaboration, A. M. Sirunyan et al., *Search for electroweak production of charginos and neutralinos in multilepton final states in proton-proton collisions at $\sqrt{s} = 13$ TeV*, *JHEP* **03** (2018) 166 [[1709.05406](#)].
- [175] CMS collaboration, A. M. Sirunyan et al., *Search for new physics in events with two soft oppositely charged leptons and missing transverse momentum in proton-proton collisions at $\sqrt{s} = 13$ TeV*, *Phys. Lett. B* **782** (2018) 440 [[1801.01846](#)].
- [176] CMS collaboration, *Search for new physics in the compressed mass spectra scenario using events with two soft opposite-sign leptons and missing momentum energy at 13 TeV*, [CMS-PAS-SUS-16-025](#).
- [177] ATLAS collaboration, *Search for supersymmetry with two and three leptons and missing transverse momentum in the final state at $\sqrt{s}=13$ TeV with the ATLAS detector*, [ATLAS-CONF-2016-096](#).
- [178] ATLAS collaboration, M. Aaboud et al., *Search for the direct production of charginos and neutralinos in final states with tau leptons in $\sqrt{s} = 13$ TeV pp collisions with the ATLAS detector*, *Eur. Phys. J. C* **78** (2018) 154 [[1708.07875](#)].
- [179] ATLAS collaboration, G. Aad et al., *Search for direct stau production in events with two hadronic τ -leptons in $\sqrt{s} = 13$ TeV pp collisions with the ATLAS detector*, *Phys. Rev. D* **101** (2020) 032009 [[1911.06660](#)].
- [180] A. Pierce, N. R. Shah and K. Freese, *Neutralino Dark Matter with Light Staus*, [1309.7351](#).

Table 5. Cutflow validation of the ATLAS analysis `atlas_2106_01676` for mass point $m(\tilde{\chi}_1^\pm/\tilde{\chi}_2^0, \tilde{\chi}_1^0) = (300, 200)$ GeV and $m(\tilde{\chi}_1^\pm/\tilde{\chi}_2^0, \tilde{\chi}_1^0) = (600, 100)$ GeV.

Process Point $m(\tilde{\chi}_2^0/\tilde{\chi}_1^\pm, \tilde{\chi}_1^0)$ Generated Events	$pp \rightarrow \tilde{\chi}_2^0 \tilde{\chi}_1^\pm, \tilde{\chi}_1^\pm \rightarrow W^\pm \tilde{\chi}_1^0, \tilde{\chi}_2^0 \rightarrow Z \tilde{\chi}_1^0$ (300, 200) GeV (600, 100) GeV 500,000			
	ATLAS	CheckMATE	ATLAS	CheckMATE
Selection				
$\mathcal{L} \times \sigma \times \text{BF}$	1760	1760	92	92
$\mathcal{L} \times \sigma \times \text{BF} \times \text{filt.eff}$	1322	1322	69	69
3 isolated leptons				
lepton $p_T^{1,2,3} > 25, 20, 10$ GeV	227	221.55	23.9	22.64
$E_T^{\text{miss}} > 50$ GeV				
$n_{\text{SFOS}} \geq 1$	226	221.55	23.7	22.64
Trigger selection	222	221.55	23.3	22.64
$n_{\text{b-jets}} = 0$	209	205.99	21.9	20.92
Resonance veto $m_{\ell\ell} > 12$ GeV	209	205.11	21.9	20.91
$ m_{3\ell} - m_Z > 15$ GeV	203	196.61	21.7	20.78
$m_{\ell\ell} \in [75, 105]$ GeV	196	187.62	20.1	19.06
$n_{\text{jets}} = 0$	76.4	82.99	7.72	7.98
$m_T \in [100, 160]$ GeV	26.7	29.19	0.9	0.97
SR^{WZ} – 1	20.9	21.25	0.09	0.12
SR^{WZ} – 2	4.86	6.93	0.11	0.14
SR^{WZ} – 3	0.78	0.78	0.16	0.15
SR^{WZ} – 4	0.14	0.23	0.54	0.55
$m_T > 160$ GeV	5.80	5.43	5.11	5.75
SR^{WZ} – 5	4.64	5.23	0.37	0.5
SR^{WZ} – 6	0.16	0.10	0.49	0.56
SR^{WZ} – 7	0	0.07	2.21	2.53
SR^{WZ} – 8	0	0	2.14	2.15
$n_{\text{jets}} > 0, H_T < 200$ GeV	97.5	91.92	9.9	9.07
$m_T \in [100, 160]$ GeV	29.6	32.82	1.19	1.13
SR^{WZ} – 9	8.75	9.90	0.17	0.18
SR^{WZ} – 10	3.46	4.45	0.32	0.35
SR^{WZ} – 11	0.54	0.36	0.15	0.15
SR^{WZ} – 12	0	0.03	0.38	0.35
$m_T > 160$ GeV	9.50	8.56	6.80	6.45
SR^{WZ} – 13	7.19	6.70	0.49	0.49
SR^{WZ} – 14	1.53	1.87	1.37	1.49
SR^{WZ} – 15	0.09	0	2.77	2.72
SR^{WZ} – 16	0	0	1.69	1.75
$n_{\text{jets}} > 0, H_T > 200$ GeV	22.2	17.33	2.40	2.25
$H_T^{\text{lep}} < 350$ GeV	20.9	16.32	0.65	0.51
$m_T > 100$ GeV	10.8	8.29	0.47	0.49
SR^{WZ} – 17	2.53	2.06	0.02	0.05
SR^{WZ} – 18	3.12	3.24	0.11	0.13
SR^{WZ} – 19	1.09	0.56	0.12	0.13
SR^{WZ} – 20	1.13	0.16	0.13	0.14

Table 6. Cutflow validation of the ATLAS analysis `atlas_2106_01676` for mass point $m(\tilde{\chi}_1^\pm/\tilde{\chi}_2^0, \tilde{\chi}_1^0) = (190, 60)$ GeV.

Process Point $m(\tilde{\chi}_2^0/\tilde{\chi}_1^\pm, \tilde{\chi}_1^0)$ Generated Events	$pp \rightarrow \tilde{\chi}_2^0 \tilde{\chi}_1^\pm, \tilde{\chi}_1^\pm \rightarrow W^\pm \tilde{\chi}_1^0, \tilde{\chi}_2^0 \rightarrow h \tilde{\chi}_1^0$ (190, 60) GeV 500,000	
	ATLAS	CheckMATE
Selection		
$\mathcal{L} \times \sigma \times \text{BF}$	10927	10927
$\mathcal{L} \times \sigma \times \text{BF} \times \text{filt.eff}$	1174	1174
3 isolated leptons		
lepton $p_T^{1,2,3} > 25, 20, 10$ GeV	192	172.23
$E_T^{\text{miss}} > 50$ GeV		
Trigger selection	186	172.23
$n_{\text{b-jets}} = 0$	171	161.34
$n_{\text{SFOS}} \geq 1$	137	122.22
Resonance veto $m_{\ell\ell} > 12$ GeV	133	114.87
$ m_{3\ell} - m_Z > 15$ GeV	110	92.51
$m_{\ell\ell} < 75$ GeV	56.2	55.74
$n_{\text{jets}} = 0$ ($\text{SR}_{\text{low-m}_{\text{ll}}-0\text{j}}^{\text{Wh}}$)	22.3	30.30
$\text{SR}_{\text{SFOS}}^{\text{Wh}} - 1$	8.26	11.03
$\text{SR}_{\text{SFOS}}^{\text{Wh}} - 2$	1.57	1.03
$\text{SR}_{\text{SFOS}}^{\text{Wh}} - 3$	0.50	0.59
$\text{SR}_{\text{SFOS}}^{\text{Wh}} - 4$	5.97	6.32
$\text{SR}_{\text{SFOS}}^{\text{Wh}} - 5$	0.64	4.41
$\text{SR}_{\text{SFOS}}^{\text{Wh}} - 6$	2.67	2.5
$\text{SR}_{\text{SFOS}}^{\text{Wh}} - 7$	2.75	4.41
$n_{\text{jets}} > 0, H_T < 200$ GeV ($\text{SR}_{\text{low-m}_{\text{ll}}-n\text{j}}^{\text{Wh}}$)	26.5	22.65
$\text{SR}_{\text{SFOS}}^{\text{Wh}} - 8$	2.95	2.50
$\text{SR}_{\text{SFOS}}^{\text{Wh}} - 9$	5.28	5.00
$\text{SR}_{\text{SFOS}}^{\text{Wh}} - 10$	1.59	2.50
$\text{SR}_{\text{SFOS}}^{\text{Wh}} - 11$	0.63	1.18
$\text{SR}_{\text{SFOS}}^{\text{Wh}} - 12$	5.55	3.23
$\text{SR}_{\text{SFOS}}^{\text{Wh}} - 13$	2.91	3.83
$\text{SR}_{\text{SFOS}}^{\text{Wh}} - 14$	0.68	0.44
$\text{SR}_{\text{SFOS}}^{\text{Wh}} - 15$	5.48	2.65
$\text{SR}_{\text{SFOS}}^{\text{Wh}} - 16$	1.39	1.32
$n_{\text{SFOS}} = 0$	34	38.82
$n_{\text{jets}} = 0$	14.8	22.80
$p_T^{\ell_3} > 15$ GeV	12.2	19.71
E_T^{miss} significance > 8	5.36	7.94
$\Delta R_{\text{OS, near}} < 1.2$	4.73	5.74
$n_{\text{jets}} \in [1, 2]$	15.6	14.56
$p_T^{\ell_3} > 20$ GeV	9.4	10.74
E_T^{miss} significance > 8	3.91	2.65
$\Delta R_{\text{OS, near}} < 1.0$	2.84	1.18
$\text{SR}_{\text{DFOS}}^{\text{Wh}}$	7.57	6.91

Table 7. Cutflow validation of the ATLAS analysis `atlas_2106_01676` for mass point $m(\tilde{\chi}_1^\pm/\tilde{\chi}_2^0, \tilde{\chi}_1^0) = (250, 170)$ GeV.

$\tilde{\chi}_1^\pm \tilde{\chi}_2^0 \rightarrow WZ \tilde{\chi}_1^0 \tilde{\chi}_1^0$ wino/bino(+)	$m(\tilde{\chi}_1^\pm/\tilde{\chi}_2^0, \tilde{\chi}_1^0) = (250, 170)$ GeV									
	ATLAS					CheckMATE				
$\mathcal{L} \times \sigma \times \text{BF}$	3559					3559				
$\mathcal{L} \times \sigma \times \text{BF} \times \text{filt.eff}$	1638					1638				
3 isolated leptons	384					434				
b veto	367					408				
Trigger	307					343				
$m_{\ell\ell}, m_{\ell\ell}^{\text{max}} [\text{GeV}]$	<75					204				
Common cuts $\text{SR}_{\text{low}E_T}^{\text{offWZ}}$	f1	f2	g1		g2	f1	f2	g1	g2	
$m_{\ell\ell}^{\text{min}} [\text{GeV}]$	[40, 75]		239					162		
lepton $P_T^{1,2,3} [\text{GeV}]$	>15		189					134		
FNP lepton cleaning			146					111		
$m_{\ell\ell}^{\text{max}} [\text{GeV}]$			146					111		
$m_{\ell\ell}^{\text{min}} [\text{GeV}]$	[40, 60]	58.2	[60, 75]		87.6		47.2		64.0	
$m_{T2}^{100} [\text{GeV}]$		58.2			87.6		47.2		64.0	
$\text{min}\Delta R$		58.2			87.6		47.2		64.0	
Cuts $\text{SR}_{\text{low}E_T}^{\text{offWZ}} - 0j$										
$n_{j\text{ets}}^{PT>30\text{GeV}}$	0	34.4	0		52.1		29.5		39.9	
$E_T^{\text{miss}} [\text{GeV}]$	<50	15.8	<50		26.6		9.7		15.7	
E_T^{miss} signif	>1.5	13.5	>1.5		22.6		9.7		15.7	
$m_{3\ell} [\text{GeV}]$	>100	10.5	>100		21.0		6.7		13.8	
$m_T^{\text{minml}} [\text{GeV}]$	<60	5.92	>90	1.57	<60	11.3	>90	3.14	2.85	1.4
$p_T^{\text{lep}}/E_T^{\text{miss}}$	<1.4	5.11	<1.4	1.44	<1.4	9.87	<1.4	2.99	2.73	1.36
Cuts $\text{SR}_{\text{low}E_T}^{\text{offWZ}} - nj$										
$n_{j\text{ets}}^{PT>30\text{GeV}}$	>0	23.7	>0		35.4		17.7		24.0	
$E_T^{\text{miss}} [\text{GeV}]$	<200	21.2	<200		31.0		15.1		20.0	
E_T^{miss} signif	>3.0	17.9	>3.0		25.2		14.3		18.9	
$m_T^{\text{minml}} [\text{GeV}]$	<60	5.88	>90	7.08	<60	8.86	>90	10.3	5.2	1.6
$p_T^{\text{lep}}/E_T^{\text{miss}}$	<1.2	4.35	<1.2	6.17	<1.2	7.15	<1.2	9.47	4.8	1.4
Cuts $\text{SR}_{\text{high}E_T}^{\text{offWZ}} - 0j$										
lepton $P_T^{1,2,3}$	[25, 15, 10]		274					202		
$m_{\ell\ell}^{\text{min}} [\text{GeV}]$	[40, 60]	91.8	[60, 75]		132		71.7		88.9	
$m_{T2}^{100} [\text{GeV}]$	<160	81.8	<175		131		63.6		87.7	
$n_{j\text{ets}}^{PT>30\text{GeV}}$	0	49.6	0		77.9		37.3		53.0	
$E_T^{\text{miss}} [\text{GeV}]$	>50	24.5	>50		37.1		23.4		32.5	
E_T^{miss} signif	>3.0	23.4	>3.0		35.5		23.4		32.5	
$m_T^{\text{minml}} [\text{GeV}]$	<70	9.62	>90	8.00	<70	14.9	>90	12.1	13.1	5.0
Cuts $\text{SR}_{\text{high}E_T}^{\text{offWZ}} - nj$										
lepton $P_T^{1,2,3}$	[4.5, 3]		299					205		
$m_{\ell\ell}^{\text{min}} [\text{GeV}]$	[40, 60]	100	[60, 75]		139		72		89.3	
$m_{T2}^{100} [\text{GeV}]$	<160	89.2	<175		138		64.3		88.0	
$n_{j\text{ets}}^{PT>30\text{GeV}}$	>0	35.6	>0		56.7		26.7		34.8	
$E_T^{\text{miss}} [\text{GeV}]$	>200	3.78	>200		7.48		4.21		6.15	
E_T^{miss} signif	>3.0	3.78	>3.0		7.35		4.21		6.15	
$p_T^{\text{lep}}/E_T^{\text{miss}}$	<1.0	3.67	<1.0		7.22		4.21		6.15	

Table 8. Cutflow validation of the ATLAS analysis `atlas_2106_01676` for mass point $m(\tilde{\chi}_1^\pm/\tilde{\chi}_2^0, \tilde{\chi}_1^0) = (125, 85)$ GeV.

$\tilde{\chi}_1^\pm \tilde{\chi}_2^0 \rightarrow WZ \tilde{\chi}_1^0 \tilde{\chi}_1^0$ wino/bino(+)	$m(\tilde{\chi}_1^\pm/\tilde{\chi}_2^0, \tilde{\chi}_1^0) = (125, 85)$ GeV											
	ATLAS						CheckMATE					
$\mathcal{L} \times \sigma \times \text{BF}$	45634						45634					
$\mathcal{L} \times \sigma \times \text{BF} \times \text{filt.eff}$	16811						16811					
3 isolated leptons	2660						3110					
b veto	2550						2961					
Trigger	1810						2051					
$m_{\ell\ell}, m_{\ell\ell}^{\text{max}}$ [GeV]	<75 1790						1867					
Common cuts $\text{SR}_{\text{low } E_T}^{\text{offWZ}}$	b		c		d		e	b	c	d	e	
$m_{\ell\ell}^{\text{min}}$ [GeV]	[12, 40]				1700					1755		
lepton $P_T^{1,2,3}$ [GeV]	>10				1440					1112		
FNIP lepton cleaning					1120					936		
$m_{\ell\ell}^{\text{max}}$ [GeV]	<60				1020					853		
$m_{\ell\ell}^{\text{min}}$ [GeV]	[12, 15]	47.0	[15, 20]	119	[20, 30]	406	[30, 40]	452	35.82	88.07	322	432
m_{T2}^{100} [GeV]	<115	19.4	<120	74.7	<130	374		452	17.91	56.02	297.06	432
$\min \Delta R$	<1.6	19.4	<1.6	73.2	<1.6	295		452	17.91	56.02	248.33	432
Cuts $\text{SR}_{\text{low } E_T}^{\text{offWZ}} - 0j$												
$n_{\text{jets}}^{PT>30\text{GeV}}$	0	12.2	0	49.5	0	186	0	291	11.73	42.29	171.05	316
E_T^{miss} [GeV]	<50	11.2	<50	42.9	<50	147	<50	242	10.31	36.13	124.48	255
E_T^{miss} signif	>1.5	8.57	>1.5	34.7	>1.5	123	>1.5	182	9.84	33.76	86.64	201
$m_{3\ell}$ [GeV]		8.57		34.7		123		182	9.84	33.76	86.64	201
m_T^{minml} [GeV]	<50	8.16	<50	32.6	<50	97.8	<60	158	6.06	21.9	54.89	151
$p_T^{\text{lep}}/E_T^{\text{miss}}$	<1.1	5.27	<1.1	22.7	<1.1	64.3	<1.3	138	5.58	21.9	39.32	123
Cuts $\text{SR}_{\text{low } E_T}^{\text{offWZ}} - nj$												
$n_{\text{jets}}^{PT>30\text{GeV}}$	>0	7.2	>0	23.8	>0	110	>0	161	6.18	13.73	77.28	116
E_T^{miss} [GeV]	<200	6.52	<200	21.3	<200	102	<200	150	6.18	13.25	75.36	113
E_T^{miss} signif	>3.0	4.72	>3.0	16.1	>3.0	76.3	>3.0	106	6.18	12.29	60.23	92.92
m_T^{minml} [GeV]	<50	2.85	<50	10.7	<50	42.9	<60	65.7	1.43	2.81	9.85	22.06
$p_T^{\text{lep}}/E_T^{\text{miss}}$	<1.0	2.54	<1.0	10.6	<1.0	36.5	<1.0	59.9	1.43	2.81	9.85	21.6
Cuts $\text{SR}_{\text{high } E_T}^{\text{offWZ}} - 0j$												
lepton $P_T^{1,2,3}$	[25, 15, 10]				1170					896		
$m_{\ell\ell}^{\text{min}}$ [GeV]	[12, 15]	44.0	[15, 20]	120	[20, 30]	422	[30, 40]	541	29.36	84.76	354	442
m_{T2}^{100} [GeV]	<115	19.1	<120	76.3	<130	388	<140	540	14.7	54.56	329	441
$n_{\text{jets}}^{PT>30\text{GeV}}$	0	11.6	0	49.6	0	239	0	341	9.93	40.29	234	306
E_T^{miss} [GeV]	>50	2.05	>50	10.3	>50	50.8	>50	67.0	1.42	7.62	60.61	72.13
E_T^{miss} signif	>3.0	1.80	>3.0	9.37	>3.0	46.1	>3.0	60.5	1.42	7.62	60.61	71.65
m_T^{minml} [GeV]	<50	1.74	<50	8.84	<60	43.3	<60	52.4	0	1.89	21.0	23.42
Cuts $\text{SR}_{\text{high } E_T}^{\text{offWZ}} - nj$												
lepton $P_T^{1,2,3}$	[4.5, 3]				1790					1867		
$m_{\ell\ell}^{\text{min}}$ [GeV]	[12, 15]	83.5	[15, 20]	207	[20, 30]	661	[30, 40]	746	94.63	222.02	744	784
m_{T2}^{100} [GeV]	<115	34.8	<130	131	<120	607	<140	744	45.15	141.84	692	782
$n_{\text{jets}}^{PT>30\text{GeV}}$	>0	15.8	>0	52.7	>0	252	>0	287	10.86	34.98	195	220
E_T^{miss} [GeV]	>200	2.09	>200	5.85	>200	22.3	>200	24.3	0	1.89	9.57	7.18
E_T^{miss} signif	>3.0	2.09	>3.0	5.85	>3.0	22.3	>3.0	24.1	0	1.89	9.57	7.18
$p_T^{\text{lep}}/E_T^{\text{miss}}$	<0.2	1.99	<0.3	5.39	<0.3	14.6	<0.3	13.8	0	1.41	4.3	4.3

Table 9. Cutflow validation of the ATLAS analysis `atlas_2106_01676` for mass point $m(\tilde{\chi}_1^\pm/\tilde{\chi}_2^0, \tilde{\chi}_1^0) = (185, 125)$ GeV.

$\tilde{\chi}_1^\pm \tilde{\chi}_2^0 \rightarrow WZ\tilde{\chi}_1^0\tilde{\chi}_1^0$ higssino	$m(\tilde{\chi}_2^0, \tilde{\chi}_1^0)=(185, 125)$ GeV											
	ATLAS						CheckMATE					
$\mathcal{L} \times \sigma \times \text{BF}$	3912						3912					
$\mathcal{L} \times \sigma \times \text{BF} \times \text{filt.eff}$	1550						1550					
3 isolated leptons	392						409					
b veto	374						388					
Trigger	280						304					
$m_{\ell\ell}, m_{\ell\ell}^{\text{max}} [\text{GeV}]$	<75						253					
	b		c		d		e		b	c	d	e
Common cuts $\text{SR}_{\text{low } E_T}^{\text{offWZ}}$												
$m_{\ell\ell}^{\text{min}} [\text{GeV}]$	[12, 40]				165						194	
lepton $P_T^{1,2,3} [\text{GeV}]$	>10				111						120	
FNIP lepton cleaning					85.2						99.9	
$m_{\ell\ell}^{\text{max}} [\text{GeV}]$	<60				79.3						92.34	
$m_{\ell\ell}^{\text{min}} [\text{GeV}]$	[12, 15]	3.53	[15, 20]	10.3	[20, 30]	32.6	[30, 40]	32.9	4.58	12.23	34.74	40.79
$m_{T2}^{100} [\text{GeV}]$	<115	0.681	<120	5.61	<130	26.3		32.9	1.41	6.14	29.70	40.79
$\min \Delta R$	<1.6	0.681	<1.6	5.55	<1.6	23.2		32.9	1.41	6.14	27.13	40.79
Cuts $\text{SR}_{\text{low } E_T}^{\text{offWZ}} - 0j$												
$n_{\text{jets}}^{PT>30\text{GeV}}$	0	0.534	0	3.84	0	13.3	0	21.3	1.05	4.36	19.31	27.78
$E_T^{\text{miss}} [\text{GeV}]$	<50	0.465	<50	2.70	<50	7.47	<50	12.8	0.68	2.43	9.88	14.05
E_T^{miss} signif	>1.5	0.465	>1.5	2.37	>1.5	6.86	>1.5	11.6	0.64	2.26	9.07	12.96
$m_{3\ell} [\text{GeV}]$		0.465		2.37		6.86		11.6	0.64	2.26	9.07	12.96
$m_T^{\text{minmll}} [\text{GeV}]$	<50	0.411	<50	2.22	<50	5.44	<60	9.46	0.64	2.06	7.78	11.35
$p_T^{\text{lep}}/E_T^{\text{miss}}$	<1.1	0.275	<1.1	1.47	<1.1	2.98	<1.3	8.04	0.40	0.85	3.51	8.08
Cuts $\text{SR}_{\text{low } E_T}^{\text{offWZ}} - nj$												
$n_{\text{jets}}^{PT>30\text{GeV}}$	>0	0.147	>0	1.71	>0	9.91	>0	11.7	0.36	1.78	7.82	13.00
$E_T^{\text{miss}} [\text{GeV}]$	<200	0.122	<200	1.54	<200	8.99	<200	10.3	0.36	1.69	7.62	12.64
E_T^{miss} signif	>3.0	0.083	>3.0	1.11	>3.0	6.84	>3.0	8.33	0.28	1.53	6.56	10.13
$m_T^{\text{minmll}} [\text{GeV}]$	<50	0.066	<50	0.886	<50	4.62	<60	5.97	0.24	0.97	4.62	7.02
$p_T^{\text{lep}}/E_T^{\text{miss}}$	<1.0	0.066	<1.0	0.783	<1.0	3.64	<1.0	4.53	0.16	0.93	3.52	5.69
Cuts $\text{SR}_{\text{high } E_T}^{\text{offWZ}} - 0j$												
lepton $P_T^{1,2,3}$	[25, 15, 10]				152						156	
$m_{\ell\ell}^{\text{min}} [\text{GeV}]$	[12, 15]	3.83	[15, 20]	11.5	[20, 30]	36.9	[30, 40]	41.9	4.87	13.17	37.52	47.27
$m_{T2}^{100} [\text{GeV}]$	<115	1.24	<120	6.19	<130	30.5	<140	40.2	1.53	6.91	32.07	45.61
$n_{\text{jets}}^{PT>30\text{GeV}}$	0	0.825	0	4.09	0	17.2	0	25.2	1.12	4.82	22.26	30.19
$E_T^{\text{miss}} [\text{GeV}]$	>50	0.205	>50	1.75	>50	8.1	>50	11.3	0.44	2.39	11.71	15.29
E_T^{miss} signif	>3.0	0.205	>3.0	1.64	>3.0	7.79	>3.0	11.0	0.44	2.39	11.71	15.29
$m_T^{\text{minmll}} [\text{GeV}]$	<50	0.205	<50	1.54	<60	7.39	<60	10.1	0.44	2.23	10.46	13.11
Cuts $\text{SR}_{\text{high } E_T}^{\text{offWZ}} - nj$												
lepton $P_T^{1,2,3}$	[4.5, 3]				253						281	
$m_{\ell\ell}^{\text{min}} [\text{GeV}]$	[12, 15]	9.76	[15, 20]	24.2	[20, 30]	65.8	[30, 40]	65.5	12.55	29.32	74.62	77.47
$m_{T2}^{100} [\text{GeV}]$	<115	3.04	<130	13.2	<120	54.0	<140	62.1	4.14	15.1	62.99	74.35
$n_{\text{jets}}^{PT>30\text{GeV}}$	>0	1.06	>0	4.50	>0	22.0	>0	22.8	1.05	5.16	19.07	24.07
$E_T^{\text{miss}} [\text{GeV}]$	>200	0.086	>200	0.613	>200	2.22	>200	2.56	0	0.12	0.48	0.78
E_T^{miss} signif	>3.0	0.086	>3.0	0.513	>3.0	2.22	>3.0	2.56	0	0.12	0.48	0.78
$p_T^{\text{lep}}/E_T^{\text{miss}}$	<0.2	0.086	<0.3	0.336	<0.3	1.44	<0.3	1.65	0	0.08	0.28	0.45

Table 10. Cutflow validation of the ATLAS analysis `atlas_2106_01676` for mass point $m(\tilde{\chi}_1^\pm/\tilde{\chi}_2^0, \tilde{\chi}_1^0) = (100, 40)$ GeV.

$\tilde{\chi}_1^\pm \tilde{\chi}_2^0 \rightarrow WZ \tilde{\chi}_1^0 \tilde{\chi}_1^0$ higssino	$m(\tilde{\chi}_2^0, \tilde{\chi}_1^0) = (100, 40)$ GeV											
	ATLAS						CheckMATE					
$\mathcal{L} \times \sigma \times \text{BF}$	48276						48276					
$\mathcal{L} \times \sigma \times \text{BF} \times \text{filt.eff}$	16084						16084					
3 isolated leptons	3760						4247					
b veto	3620						4027					
Trigger	2620						3165					
$m_{\ell\ell}, m_{\ell\ell}^{\text{max}} [\text{GeV}]$	<75						2916					
Common cuts $\text{SR}_{\text{low } E_T}^{\text{offWZ}}$	b		c		d		e	b	c	d	e	
$m_{\ell\ell}^{\text{min}} [\text{GeV}]$	[12, 40]				1590					2012		
lepton $P_T^{1,2,3} [\text{GeV}]$	>10				1050					1241		
FNIP lepton cleaning					820					1037		
$m_{\ell\ell}^{\text{max}} [\text{GeV}]$	<60				770					958		
$m_{\ell\ell}^{\text{min}} [\text{GeV}]$	[12, 15]	36.6	[15, 20]	101	[20, 30]	302	[30, 40]	331	47.55	126.89	361	423
$m_{T2}^{100} [\text{GeV}]$	<115	15.6	<120	59.1	<130	262		331	14.65	63.72	308	423
$\min \Delta R$	<1.6	15.6	<1.6	58.6	<1.6	216		331	14.65	63.72	282	423
Cuts $\text{SR}_{\text{low } E_T}^{\text{offWZ}} - 0j$												
$n_{jets}^{PT>30\text{GeV}}$	0	11.5	0	43.7	0	149	0	216	10.86	45.29	200	288
$E_T^{\text{miss}} [\text{GeV}]$	<50	10.1	<50	32.9	<50	103	<50	161	7.09	25.17	103	146
E_T^{miss} signif	>1.5	8.03	>1.5	29.2	>1.5	92.6	>1.5	134	6.67	23.49	94.17	135
$m_{3\ell} [\text{GeV}]$		8.03		29.2		92.6		134	6.67	23.49	94.17	135
$m_T^{\text{minml}} [\text{GeV}]$	<50	7.41	<50	26.8	<50	80.2	<60	118	6.67	21.40	80.76	118
$p_T^{\text{lep}}/E_T^{\text{miss}}$	<1.1	5.94	<1.1	8.0	<1.1	50.4	<1.3	100	4.16	8.82	36.37	83.87
Cuts $\text{SR}_{\text{low } E_T}^{\text{offWZ}} - nj$												
$n_{jets}^{PT>30\text{GeV}}$	>0	4.12	>0	14.9	>0	67.6	>0	115	3.78	18.43	81.13	135
$E_T^{\text{miss}} [\text{GeV}]$	<200	4.12	<200	14.5	<200	64.9	<200	111	3.78	17.59	79.03	131
E_T^{miss} signif	>3.0	2.81	>3.0	10.9	>3.0	45.6	>3.0	76.4	2.95	15.92	68.09	105
$m_T^{\text{minml}} [\text{GeV}]$	<50	1.96	<50	9.16	<50	34.2	<60	60.9	2.52	10.05	47.91	72.83
$p_T^{\text{lep}}/E_T^{\text{miss}}$	<1.0	1.68	<1.0	7.34	<1.0	27.6	<1.0	44.4	1.69	9.64	36.57	58.96
Cuts $\text{SR}_{\text{high } E_T}^{\text{offWZ}} - 0j$												
lepton $P_T^{1,2,3}$	[25, 15, 10]				1350					1621		
$m_{\ell\ell}^{\text{min}} [\text{GeV}]$	[12, 15]	37.1	[15, 20]	102	[20, 30]	313	[30, 40]	396	50.53	137	389	491
$m_{T2}^{100} [\text{GeV}]$	<115	16.1	<120	63.0	<130	269	<140	382	15.89	71.76	333	473
$n_{jets}^{PT>30\text{GeV}}$	0	11.8	0	46.6	0	184	0	252	11.67	50.00	231	313
$E_T^{\text{miss}} [\text{GeV}]$	>50	1.23	>50	16.7	>50	68.2	>50	75.9	4.6	24.77	122	159
E_T^{miss} signif	>3.0	1.13	>3.0	16.2	>3.0	65.0	>3.0	72.5	4.6	24.77	122	159
$m_T^{\text{minml}} [\text{GeV}]$	<50	1.13	<50	16.2	<60	62.8	<60	68.5	4.6	23.11	109	136
Cuts $\text{SR}_{\text{high } E_T}^{\text{offWZ}} - nj$												
lepton $P_T^{1,2,3}$	[4.5, 3]				2380					2916		
$m_{\ell\ell}^{\text{min}} [\text{GeV}]$	[12, 15]	99.4	[15, 20]	233	[20, 30]	621	[30, 40]	640	130	304	774	804
$m_{T2}^{100} [\text{GeV}]$	<115	42.4	<130	140	<120	537	<140	617	43.01	157	654	772
$n_{jets}^{PT>30\text{GeV}}$	>0	12.0	>0	37.0	>0	162	>0	200	10.89	53.57	198	250
$E_T^{\text{miss}} [\text{GeV}]$	>200	0.376	>200	1.07	>200	7.12	>200	7.30	0	1.27	5.02	8.04
E_T^{miss} signif	>3.0	0.376	>3.0	1.07	>3.0	6.95	>3.0	7.30	0	1.27	5.02	8.04
$p_T^{\text{lep}}/E_T^{\text{miss}}$	<0.2	0.146	<0.3	0.771	<0.3	4.37	<0.3	3.07	0	0.84	2.92	4.65